AD-A111 141 AIR FORCE INST OF TECH WRIGHT-PATTERSON AFB OH SCHOO--ETC F/G 20/10
INVESTIGATION OF LASER INDUCED FLUORESCENCE FOR CONCENTRATION M--ETC(U)
DEC 81 T R ROBBINS
UNCLASSIFIED AFIT/GEP/PH/81D-8 NL

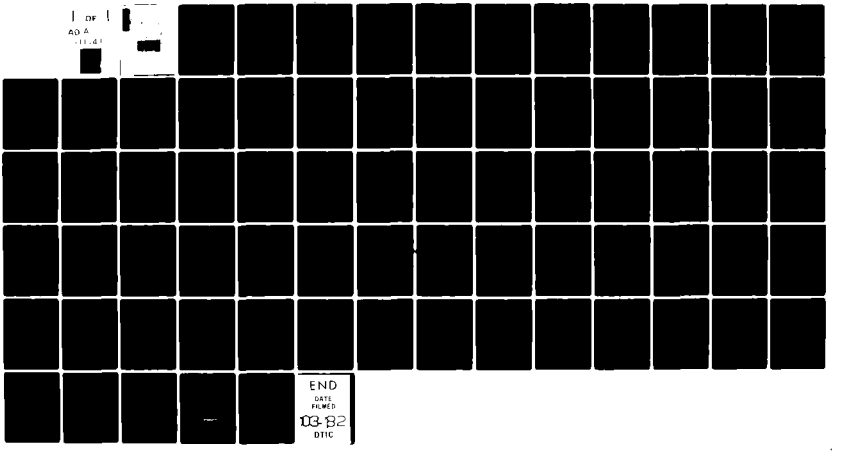

END
DATE FILMED
03-82
DTIC

AFIT/GEP/PH/81D-8

INVESTIGATION OF LASER INDUCED FLUORESCENCE FOR CONCENTRATION MEASUREMENTS OF DIATOMIC SULFUR

THESIS

AFIT/GEP/PH/81D-8

Tyrie R. Robbins
Captain USAF

AFIT/GEP/PH/81D-8

INVESTIGATION OF LASER INDUCED FLUORESCENCE FOR CONCENTRATION MEASUREMENTS OF DIATOMIC SULFUR

THESIS

Presented to the Faculty of the School of Engineering

of the Air Force Institute of Technology

Air University

in Partial Fulfillment of the

Requirements for the Degree of

Master of Science

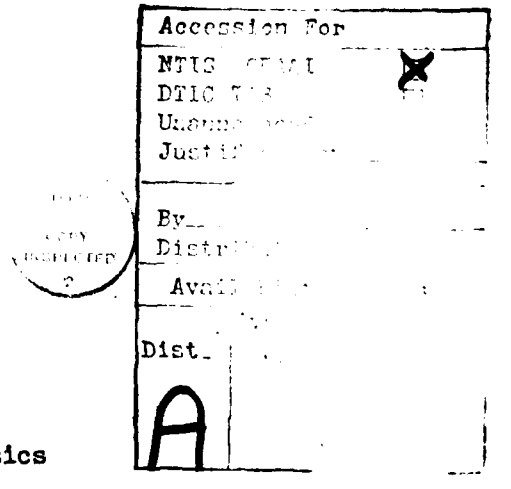

by

Tyrie R. Robbins

Captain USAF

Graduate Engineering Physics

December 1981

Approved for public release; distribution unlimited

Preface

This thesis was a challenging and demanding experience, the long hours of experimenting and writing well worth it upon completion. I am especially grateful for the opportunity to "learn by doing" this work presented, allowing me to experience firsthand the laboratory environment.

My deepest thanks go to Dr. Paul Schreiber of the Air Force Aero Propulsion Laboratory and Dr. Won B. Roh of the Air Force Institute of Technology Physics Department for jointly developing this project and making it available. Dr. Schreiber expertly laid the foundation for the work, while Dr. Roh was a superb advisor whose detailed knowledge and extensive background provided me with a sincere appreciation of experimental research.

I would like to thank the Aero Propulsion Laboratory for sponsoring this thesis, and for the people, facilities, and equipment they provided. I am especially grateful to Sig Kizirnis for all his help in getting me started and teaching me how to use the equipment; to Don Linder for keeping the equipment working properly; to Jimmy Ray for making the sample tubes; and to Bob Brecha from Wright State University for his full-time help and for being such an able-bodied lab assistant.

Finally, I wish to thank my wife Caroline for her patience, understanding, and encouragement throughout this period, and for her typing and improvements of the written report.

Contents

List of Illustrations

List of Symbols

Roman Letters

°C	Degrees centigrade
E	Energy (joules)
exp	Exponential of the quantity following
h	Planck's constant
Hz	Hertz (cycles or pulses per second)
k	Boltzmann's constant
°K	Degrees Kelvin
P	Pressure (torr)
PIN	Photodiode constructed of a p-type region, intrinsic region, and n-type region
t	Time
T	Temperature (°K)
UV	Ultraviolet
v'	Vibrational quantum number - excited electronic state
v"	Vibrational quantum number - ground electronic state

Greek Letters

Δ	Difference or change
ν	Frequency (Hz)
Σ	Summation of the quantity following

Units of Measure

Concentration

ppm	Parts per million

Current

mA	Milliampere

Energy

J	Joules

Length

m	Meter
cm	Centimeter
mm	Millimeter
μ	Micron (micrometer)
nm	Nanometer
Å	Angstrom (10^{-10} meter)

Power

kW	Kilowatt
mW	Milliwatt

Time

min	Minute
sec	Second
msec	Millisecond
μsec	Microsecond
nsec	Nanosecond

Voltage

V	Volt
mV	Millivolt

Note: Other specific symbols are defined where they first occur in Sections III and VI.

Abstract

The technique of laser induced fluorescence was used to measure S_2 number densities in a laboratory environment. A rate equation analysis was performed to model transitions within the $B^3\Sigma_u^- - X^3\Sigma_g^-$ system. The $v' = 2$, $v'' = 3$ transition in S_2 at 3290.7 Å was selected for nonresonance fluorescence studies, which included broad spectrum identification, fluorescence intensity versus temperature and laser power measurements, effective lifetime measurements, and total number density calculations. Data was taken near 600°C to ensure that a large percentage of the sulfur vapor was S_2 ($\geq$ 98%). A pulsed nitrogen laser operating at 3371 Å served as the excitation source for this experiment. Pumping in S_2 occured over the $v' = 2$, $v'' = 4$ transition at 3369 Å due to its near overlap with the N_2 laser line. Experimentally determined number densities were too large in the low pressure region, but generally within one order of magnitude over the 0.3 to 12.6 torr range examined. In concept, laser induced fluorescence proved to be a feasible means of measuring S_2 concentrations. Differences between the known and calculated number densities are attributed to the complexity of S_2, quenching and radiation trapping, difficulties in measuring the effective lifetime, and inadequacies in the rate equation model.

INVESTIGATION OF LASER INDUCED FLUORESCENCE FOR CONCENTRATION MEASUREMENTS OF DIATOMIC SULFUR

I. Introduction

Background

Over the past several decades, diatomic sulfur (S_2) gas has been the subject of intense theoretical and experimental investigations. As a result, researchers have acquired greater knowledge of the electronic energy levels and transitions within the sulfur molecule. By applying this knowledge, several scientists recently produced stable discharges and lasing using S_2 (Refs 18, 21, and 28). The placement of energy levels suggests that a very efficient and high-power S_2 laser could be developed, having an output beam tunable from visible through ultraviolet wavelengths (Refs 1, 18, 21 and 28).

For laser applications, a rate equation analysis must be performed to determine sulfur's suitability as a lasing medium and to estimate the efficiency with which it would operate. In a molecule such as S_2, this analysis is complicated by the large number of energy levels and transitions between these levels. Prominent transitions must be selected and studied individually in order to provide useful information.

Once a specific transition is identified, the rate equations can be used to describe interactions between various energy levels. The strength or lasing response of a transition depends directly on the population difference between the upper and lower energy levels responsible for it (Ref 25:181). By knowing the total number density, the rate equations can be used to calculate individual level populations,

allowing further determination of sulfur's lasing potential. Thus, the task is to measure total S_2 number densities through experimental means, then compare these results to known values.

There are a variety of optical diagnostic techniques currently being used to measure species concentrations in gases. Four of the most common techniques include:

1. absorption spectroscopy;
2. spontaneous Raman scattering;
3. coherent anti-Stokes Raman scattering (CARS);
4. laser induced fluorescence.

Each of these methods will be discussed in greater detail in Section II.

Problem

The problem for this thesis is to investigate the feasibility of using laser induced fluorescence to measure total S_2 number densities in a laboratory environment. The theoretical model describing these transitions is developed and compared to the experimental results.

General Approach

Equipment was acquired and set up as described in Section IV. Broad spectra were first taken to find the S_2 lines and activity identified in earlier works. Strong emission lines were selected for further study and scanned in detail with improved resolution. Data from these lines was analysed and compared to theoretical predictions.

Presentation

Section II examines the four diagnostic techniques, briefly describing their advantages and disadvantages. In Section III, the theory of laser induced fluorescence is developed and used to model

selected S_2 transitions. Section IV describes the equipment and experimental set-up, while Section V outlines the procedure followed. Section VI presents the results of this experiment and discusses them in light of theory. A brief summary, main conclusions, and recommendations for future research are contained in Section VII.

II. Diagnostic Techniques

The advent of the laser has enabled optical diagnostic techniques to assume an ever-increasing role in the broad spectrum of physical investigations. In the past, gas parameters such as temperature and species concentration were determined using material probes, but not without great difficulty. Material probes, although simple and inexpensive, suffered because their temporal response was poor; their size limited the spatial resolution obtainable; they disturbed the medium; and they were susceptible to damage when placed in a hostile environment (Ref 24:1). Optical probes, on the other hand, provide enhanced non-disturbing, remote, and point probing capabilities.

Though some laser diagnostic systems may be large and expensive, they are ideally suited to laboratory use. Four of the most common optical diagnostic techniques are discussed in this section. These are: (1) absorption spectroscopy, (2) spontaneous Raman scattering, (3) coherent anti-Stokes Raman scattering (CARS), and (4) laser induced fluorescence. The basic principles of each technique will be examined, along with their advantages and disadvantages. The reasons for choosing laser induced fluorescence will also be discussed.

Absorption Spectroscopy

In absorption spectroscopy, the gas sample is irradiated with a beam of laser light at frequency ν. The frequency is tuned so that it corresponds to a transition having an upper and lower energy state difference ΔE, where $\Delta E = h\nu$. This condition causes the molecule to absorb energy from the beam and jump from the lower energy level to the higher energy level (Ref 2:6). A detector collecting the radiation

after it passes through the sample will register a decrease in beam intensity. In order to calculate desired parameters, this decrease can be compared to a known value or reference beam that by-passes the sample. If a broad band illumination source containing a wide range of frequencies is used instead of the laser, intensity decreases will result for all frequencies that correspond to characteristic energy differences and transitions within the molecule. An absorption spectrum is produced that can be recorded on chart paper or photographic film.

The main advantage of absorption spectroscopy is the lack of complicated equipment required to obtain absorption spectra. The major disadvantage lies in the fact that measurements are averaged over certain path lengths, and therefore do not yield spatially resolved results (Ref 12:9).

Spontaneous Raman Scattering

Spontaneous Raman scattering results from the inelastic scattering of radiation from atoms or molecules. During an inelastic collision, energy is exchanged according to the molecule's energy quantization laws. The change in energy, ΔE, must equal the difference in energy between two of its allowed states, representing a change in vibrational or rotational energy.

To describe the Raman process, consider the molecule's interaction with a photon of energy $h\nu$. If the molecule gains energy ΔE, the photon will be scattered with decreased energy $h\nu - \Delta E$ at a lower frequency $\nu' = \nu - \Delta E/h$. This phenomena is known as Raman Stokes scattering (Ref 12:54). On the other hand, if the molecule loses energy ΔE, the photon will be scattered with increased energy $h\nu + \Delta E$ at a higher corresponding frequency $\nu' = \nu + \Delta E/h$. This last event

occurs when the molecule is in an excited state prior to the collision and is called Raman anti-Stokes scattering. Stokes radiation is usually more intense than anti-Stokes radiation since most molecules exist naturally in ground or lower energy states (Ref 2:122).

Spontaneous Raman techniques possess several advantages over other diagnostic methods. First, only a single laser is required. This laser can operate at any wavelength and does not need to be tuned to resonance frequencies of the molecule being probed (Ref 12:53). Also, several species can be monitored simultaneously, the observed intensities not affected by quenching. Finally, spontaneous Raman scattering can be used to study rotations and vibrations of molecules which do not produce infrared or microwave spectra, or which are inaccessible to infrared and microwave techniques.

The major disadvantage of spontaneous Raman scattering and the one which limits its use is that Raman signals are very weak (Ref 12:53). The weakness of Raman spectra result in very low signal to noise ratios and poorer resolution capabilities, especially in observing rotational fine structure. In the majority of cases, spontaneous Raman spectroscopy is used to compliment other techniques in areas where they are limited.

Coherent Anti-Stokes Raman Scattering

Coherent anti-Stokes Raman scattering (CARS) is a nonlinear optical process involving two laser sources. The pump frequency ν_1 and the Stokes frequency ν_2 are selected such that $\nu_1 - \nu_2$ is tuned to the vibrational frequency of a Raman active resonance. The sample being examined then emits strong radiation at the anti-Stokes frequency $\nu_3 = 2\nu_1 - \nu_2$. In contrast to other techniques, CARS radiation

occurs in a well-defined, phase-matched direction, producing a very coherent beam (Ref 24:11). This beam is also confined to an extremely small solid angle, making signal collection very efficient.

Thus, the main advantage of the CARS technique is that the anti-Stokes signal is very intense, nearly all of which can be collected. The CARS signal-to-noise ratio is also several orders of magnitude stronger than the corresponding spontaneous Raman signal (Ref 13:12). Discrimination against background radiation and laser induced fluorescence effects is greatly enhanced because of these properties. With the development of tunable dye lasers, the CARS technique is now receiving greater attention in the areas of high-resolution spectroscopy, analytical chemistry, and gas diagnostics.

The major disadvantage of CARS diagnostics is that two lasers are needed. The resulting experimental set-up is usually complicated and very sensitive to optical alignment (Ref 29:2). Analysis often requires complex data reduction and necessitates computer support.

Laser Induced Fluorescence

Laser induced fluorescence is the process of exciting molecules to higher energy levels with light on an appropriate frequency, then observing the radiation emitted in their decay to lower energy levels. This process is illustrated in Figure 1 on the next page. Resonance fluorescence occurs when the emitted frequency is equal to that of the incident frequency. If the molecule decays to energy levels other than the original one, there is a corresponding frequency shift in the emitted radiation, known as non-resonance fluorescence. The time between initial absorption and return to the ground state is usually very small, with fluorescence lifetimes varying between 10^{-10} and 10^{-5}

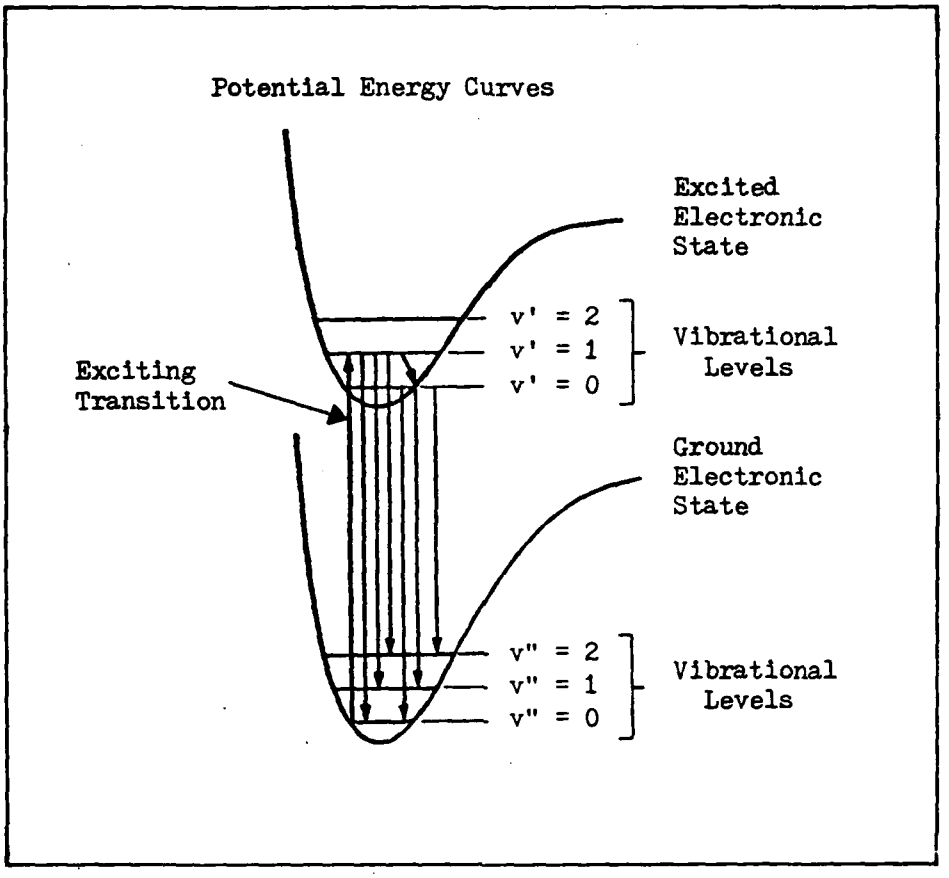

Figure 1. Laser Induced Fluorescence (Ref 24:3)

seconds (Ref 12:8).

Laser induced fluorescence possesses several advantages over other diagnostic techniques. First, fluorescence cross sections and resulting emission signals are generally many orders of magnitude stronger than those from the spontaneous Raman method. Sensitivity is also higher than that obtainable through the CARS method. Secondly, non-resonance or shifted fluorescence wavelengths can be examined to avoid interference from laser scattering or competing mechanisms. The strength of the fluoresence signal is linearly dependent on the excited

state species concentration corresponding to that particular wavelength (Ref 29:4). Finally, equipment needs for laser induced fluorescence are less and the experimental set-up usually simpler.

The main disadvantage of laser induced fluorescence is that the emitted signal is often affected by other nonradiative processes. These processes are collectively called quenching, and include: dissociation; chemical reactions; energy transfer to other internal states within the molecule of interest; and energy transfer to other molecules through collisions (Ref 12:8). Quenching effects reduce the intensity of the fluorescence signal and cause the total decay rate to increase. In order to correct for these effects, the number densities and quenching rates of each molecule must be known. To minimize the impact of quenching processes, the techniques of saturated or near-saturated laser induced fluorescence are often used (Refs 3, 4, 7, 8, and 22).

Selection of Laser Induced Fluorescence

The first step in evaluating sulfur's potential as a laser is to develop a method to measure S_2 concentrations. After reviewing current literature on S_2, laboratory equipment available, time constraints, and the four optical diagnostic techniques discussed in this section, it was determined that laser induced fluorescence would be investigated for this thesis. The reasons for selecting this method include:

1. The stronger signal produced by laser induced fluorescence than by spontaneous Raman scattering, and the higher sensitivity achievable than with CARS.
2. The simpler experimental set-up and availability of needed equipment (see Section IV).

3. The multitude of S_2 energy levels and transitions available, providing more flexibility in selecting wavelengths to examine (see Ref 21, Tables III-V, pp. 1559-1561).

4. The small amounts of other species at planned operating temperatures of 600°C and pressures less than 20 torr. These two factors should combine to minimize quenching effects that would occur under less favorable conditions.

Overall, laser induced fluorescence appeared to offer more advantages over other methods. Therefore, this thesis will investigate the feasibility of using laser induced fluorescence to measure S_2 concentrations.

III. Theory

In this section, the theory behind the experimental method will be discussed. Laser induced fluorescence is examined in detail, with the overall goal to develop a quantitative relationship that gives the total number of S_2 molecules as a function of the observed fluorescence intensity. The discussion is divided into the following main topics: (1) rate equations, (2) assumptions and approximations, (3) solution to the rate equation, (4) observed fluorescence intensity, (5) experimental considerations, and (6) sulfur vapor composition.

Rate Equations

As discussed in the previous section, laser induced fluorescence is the process of exciting molecules to higher energy levels with light of an appropriate frequency, then observing the radiation emitted in their decay to lower energy levels. Since the strength of the fluorescence signal is directly proportional to the number of molecules in the excited state, a model is needed to describe the population changes and energy transfers that occur. The rate equation model embodies these concepts, and can vary from the simple two-level to three-, four-, or even multi-level models. As additional energy levels and their interactions are considered, the complexity of the model increases and calculations become correspondingly more difficult. To perform a complete and rigorous quantum-mechanical analysis on a large collection of multi-level atoms or molecules, the quantum-mechanical density-matrix approach is most often used (Ref 25:249). The density-matrix approach treats the state of each system in a statistical manner, providing a more exact analysis (Refs 9, 11, and 28).

The theory presented here is developed using the rate equations, since the density-matrix approach is beyond the scope of this work. The rate equations also give fairly accurate solutions and agree well with observed phenomena when the system is initially in thermal equilibrium (Ref 25:253). In this analysis, only the $B^3\Sigma_u^- - X^3\Sigma_g^-$ system in S_2 is modeled. The approximate potential energy curves (PEC's) for this system are shown in Figure 2 on the next page. The $X^3\Sigma_g^-$ ground molecular state is formed from two ground state sulfur atoms, while the $B^3\Sigma_u^-$ excited state originates from one excited ^1D sulfur atom and one ground state sulfur atom. The molecular PEC's are displaced in their relative internuclear position so that the lowest vibrational levels of the $B^3\Sigma_u^-$ state lie above high vibrational levels of the $X^3\Sigma_g^-$ ground state. The $v' \leq 9$ vibrational levels of the $B^3\Sigma_u^-$ state are also bound and strongly perturbed (Ref 21:1553). Within this system, the $v' = 2$, $v'' = 3$ transition at 3290.7 Å was selected for detailed study.

To describe interactions of the $v' = 2$, $v'' = 3$ transition, a three-level model is developed. This model is shown in Figure 3 on page 14, the energy levels labeled with their actual vibrational quantum numbers. The rotational sub-structure of each vibrational level will not be considered in this analysis, due in part to the lack of resolution needed to distinguish rotational fine structure in the fluorescence spectra. In reality, rotational effects are important, especially since they exhibit strong temperature dependence.

The thermal distribution of rotational levels is governed not only by a Boltzmann factor, but by a degeneracy factor as well. This degeneracy is equal to $(2J + 1)$ where J is the rotational quantum

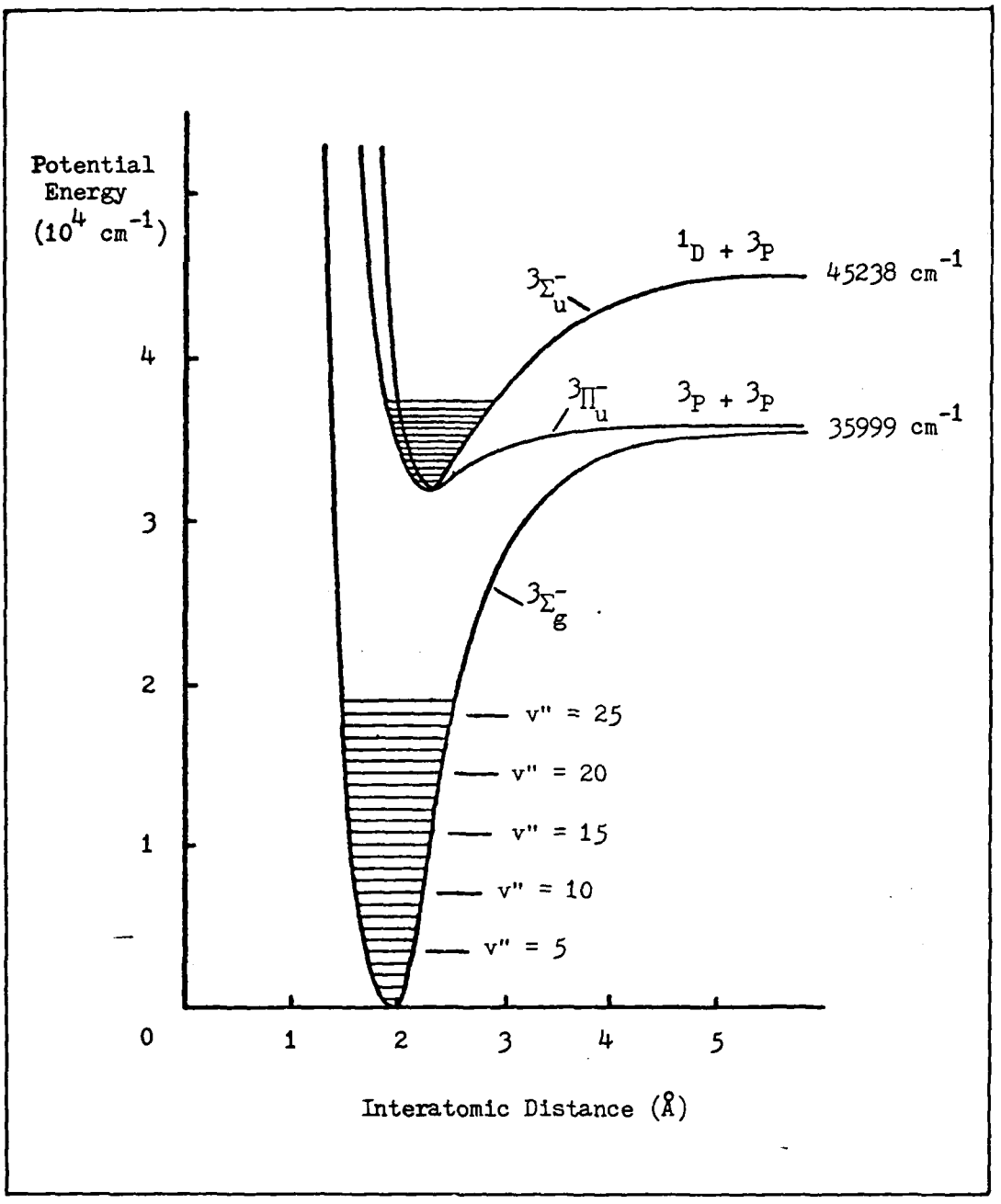

Figure 2. Approximate S_2 Potential Energy Curves (Ref 20:10)

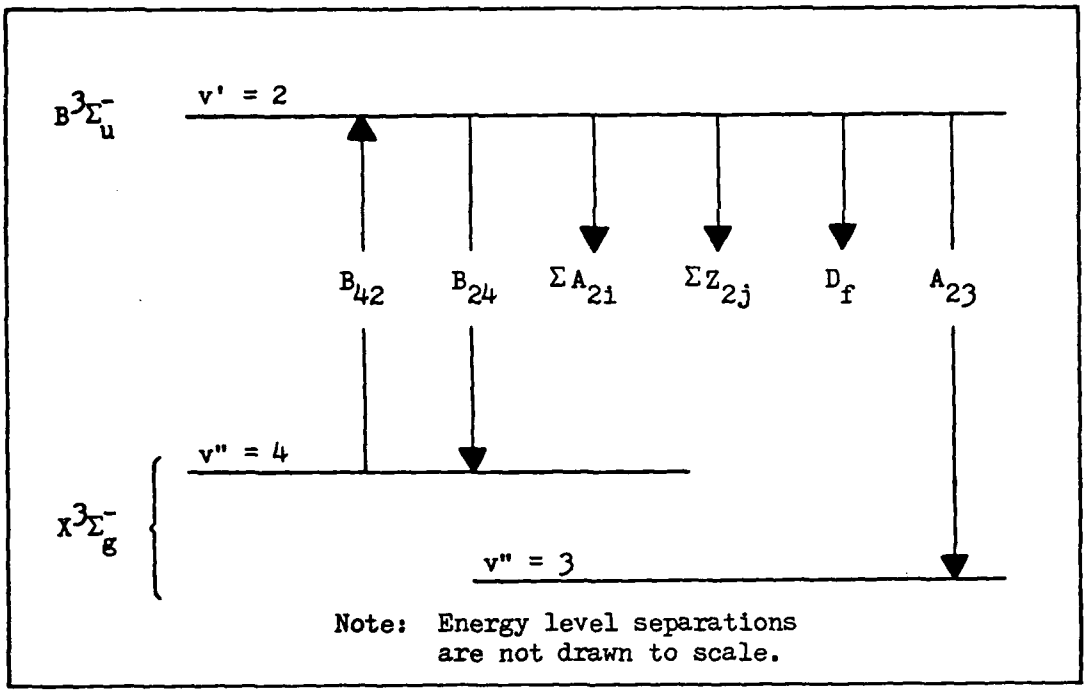

Figure 3. Three-level Model

number. The number of molecules $N_{J,v}$ in any particular vibrational-rotational state is then given by (Ref 16:123-125):

$$N_{J,v} = N_e \left[\frac{g_v}{Z_v} \exp(-E_v/kT)\right]\left[\frac{(2J+1)}{Z_J} \exp(-E_J/kT)\right] \qquad (1)$$

vibrational effects | rotational effects

where N_e = total number density for a given electronic state

g_v = vibrational degeneracy (g_v = 1 for a diatomic molecule)

Z_v = vibrational partition function

E_v = vibrational energy

$(2J + 1)$ = rotational degeneracy

Z_J = rotational partition function

E_J = rotational energy

Since the degeneracy factor $(2J + 1)$ increases linearly with J, the number of molecules in the different rotational levels first goes through a maximum before it begins to decrease. This maximum is given by the expression (Ref 16:124):

$$J_{max} = 0.5896\sqrt{T/B} - \tfrac{1}{2} \qquad (2)$$

where T = the temperature (°K)

B = the molecule's rotational constant (cm^{-1})

When considering transitions between two vibrational states, the number and placement of rotational levels affected depends upon the bandwidth of the phenomena causing the transition and the gas temperature at which the transition occurs. This rotational distribution is important in both the pumping of molecules to excited energy levels and in their decay to lower energy levels. These considerations are illustrated in Figure 4 on the following page. To a first approximation, the variation in intensity of vibrational-rotational lines is proportional to Equation (1). However, due to the transition bandwidth uncertainties encountered in this experiment and other factors that complicate the theory, rotational effects will not be quantitatively included. Their

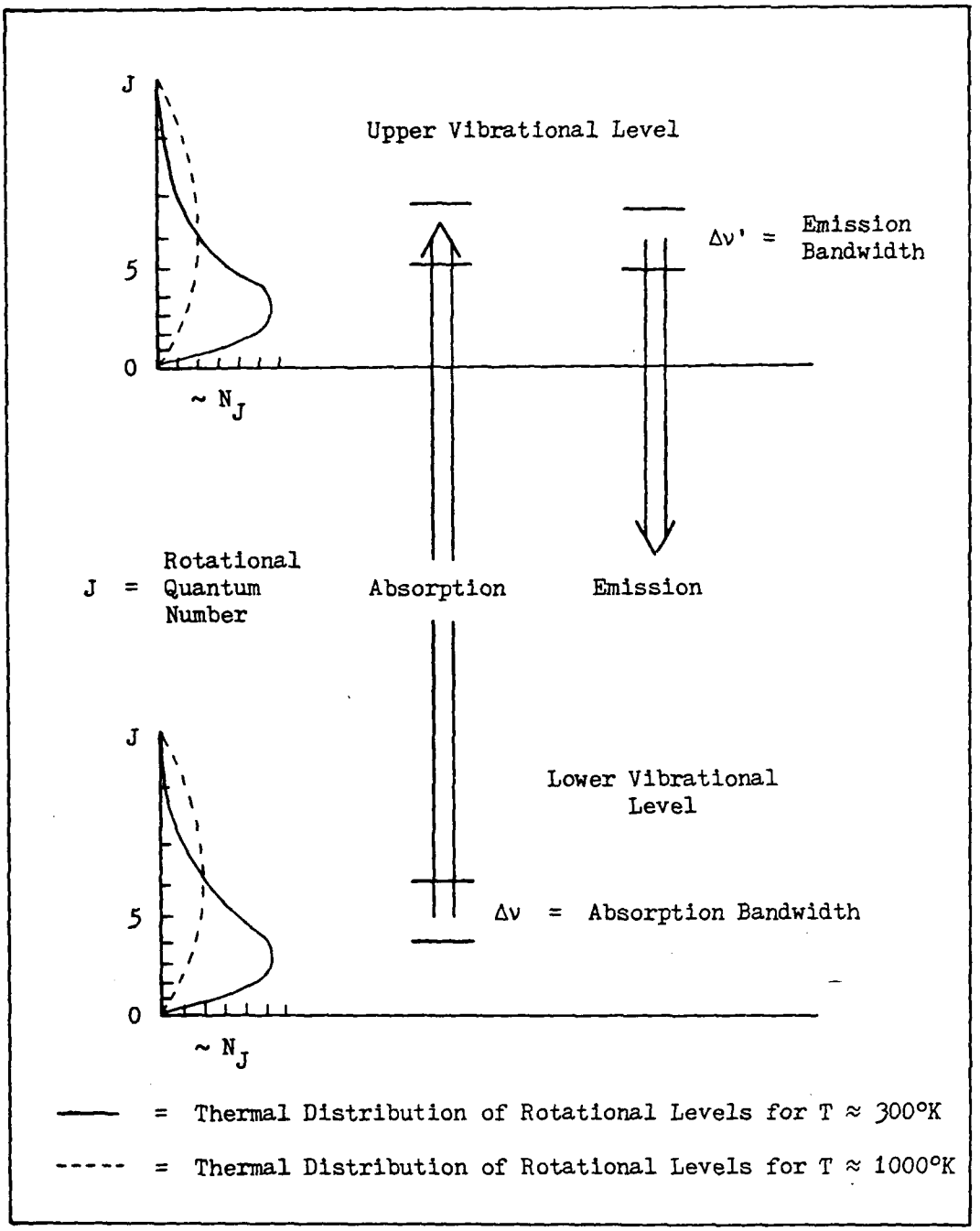

Figure 4. Thermal Distribution of Rotational Levels (Ref 16:124-125)

possible impact upon the results will be discussed in general terms in Section VI.

With this introduction, the rate equations for the three-level model can be developed. In this analysis, only the equation for the $v' = 2$ level will be considered. Referring to Figure 3, the change in population with time for this level is given by:

$$\frac{dN_2(t)}{dt} = B_{42}\rho(\nu)N_4(t) - B_{24}\rho(\nu)N_2(t) - A_{23}N_2(t) - \sum_{\substack{i \\ i \neq 3}} A_{2i}N_2(t) - \sum_j Z_{2j}N_2(t)N_j(t) - D_f\nabla^2 N_2(t) \quad (3)$$

where B_{42} = integrated Einstein B coefficient for stimulated absorption (m^3/joules-sec^2)

B_{24} = integrated Einstein B coefficient for stimulated emission (m^3/joules-sec^2)

A_{23} = Einstein A coefficient for spontaneous emission from the $v' = 2$ to the $v'' = 3$ energy level (sec^{-1})

A_{2i} = Einstein A coefficient for spontaneous emission from the $v' = 2$ to $v'' = i$ energy levels (sec^{-1})

Z_{2j} = collisional rate constant (m^3/sec)

D_f = diffusion coefficient (sec^{-1})

$N_4(t)$ = number density of molecules in the $v'' = 4$ vibrational level (m^{-3})

$N_2(t)$ = number density of molecules in the $v' = 2$ vibrational level (m^{-3})

$N_j(t)$ = colliding molecule number density for each of the j species (m^{-3})

$\rho(\nu)$ = laser energy density (joules/m^3-Hz)

Equation (3) can be simplified somewhat by letting

$$\sum_{\substack{i \\ i \neq 3}} A_{2i} = A_2 \qquad \text{and} \qquad \sum_j Z_{2j} N_j(t) = Q_2 \tag{4}$$

where A_2 represents the total spontaneous decay rate from the upper level to all lower levels except the one of interest, and Q_2 represents the total quenching (nonradiative) relaxation rate. With these simplifications, Equation (3) becomes

$$\frac{dN_2(t)}{dt} = B_{42}\rho(\nu)N_4(t) - B_{24}\rho(\nu)N_2(t) - (A_{23} + A_2 + Q_2)N_2(t) - D_f\nabla^2 N_2(t) \tag{5}$$

To analyze a system containing M different energy levels, the rate equations are first developed for each level in the manner described above. These form a set of M coupled differential equations, M - 1 of which are linearly independent. The additional Mth equation needed to complete the set is given by the population condition: $\sum_i N_i(t) = N_{Total}$. The populations for each of the M levels can then be determined by solving the full set of rate equations. The only drawback to this approach lies in the fact that the general solutions are algebraically involved even for the three-level case, and are extremely lengthy for more complicated systems with larger numbers of energy levels (Ref 25:254). To apply this model without solving the entire system of equations, simplifications must be made to allow use of each rate equation individually. These simplifications will be

discussed in the next few paragraphs.

Assumptions and Approximations

To facilitate greater use of the rate equations in experimental analyses, several assumptions can be made. The foremost of these assumes steady state operation where all time derivatives are set equal to zero. The rate equations can then be solved as a system of linear equations in M unknowns. Even though the steady state condition is applicable to many laser analyses (Ref 27:3-24), it does not accurately describe diagnostic situations occuring on very short time scales. The latter was true in this experiment. The population $N_2(t)$ increased while the laser pulse was on, then rapidly decreased after the laser pulse ended. Due to the transient nature of $N_2(t)$, the time dependence in Equation (5) had to be retained.

Another prominent assumption relates to saturation of the absorbing transition through use of pulsed lasers with high spectral intensity. Saturation is the condition under which stimulated absorption and emission completely dominate other processes (Ref 12:77). Daily and Piepmeier have shown that the observed fluorescence intensity is independent of both quenching and laser power under saturation conditions (Refs 7, 8, 10 and 22). If full saturation cannot be achieved, partial saturation conditions still allow some simplification. Baronavski and McDonald have shown that under near-saturation, fluorescence intensity versus laser power measurements will yield the total quenching rate and upper level number density (Refs 3 and 4). As with the steady state assumption, it must be known whether or not experimental phenomena exhibit saturation behavior. To test for saturation conditions, fluorescence intensity versus laser power must be

measured. In this experiment, these measurements produced a linear, straight line relationship (see Section VI), indicating even partial saturation was not achieved.

Since S_2 did not exhibit steady state or saturation conditions, other means of simplifying Equation (5) were needed. Thermal equilibrium does apply to this experiment on both the microscopic and macroscopic levels, thus allowing further approximations. On a microscopic level, before the laser pulse occurs, sulfur molecules are in thermal equilibrium near 600°C. According to statistical mechanics, the relative populations N_j and N_i of any two energy levels E_j and E_i must be related by the Boltzmann equation (Ref 25:18):

$$\frac{N_j}{N_i} = \exp[-(E_j - E_i)/kT] = \exp(-\Delta E/kT) \qquad (6)$$

Near 600°C, the thermal energy kT corresponds to an energy gap of approximately 417 cm^{-1}, while the energy difference ΔE between the $X^3\Sigma_g^-$ ground electronic state and the $B^3\Sigma_u^-$ excited electronic state in S_2 is roughly 3.2×10^4 cm^{-1}. Under these conditions, $\Delta E \gg kT$ and $\exp(-\Delta E/kT) \approx 0$, implying that all molecules are in the ground electronic state. Since the laser energy density is a very small number and conditions are far from saturation, only a minute fraction of these molecules will be pumped to the $v' = 2$ level compared to $N_4(t)$. In addition, the stimulated emission term $B_{24}\rho(\nu)N_2(t)$ will be even smaller because it contains both $\rho(\nu)$ and $N_2(t)$. Therefore, compared to the processes of quenching and spontaneous emission, stimulated emission will be negligible and can be disregarded for this analysis.

Also on a microscopic scale, molecules of the $v'' = 4$ level are in thermal equilibrium with molecules in the other vibrational levels of the ground electronic state. Compared to this thermal distribution, the process of stimulated absorption and spontaneous emission will not appreciably affect the total population of the $v'' = 4$ level. $N_4(t)$ can be approximated as a constant, N_4, and related to the total number of S_2 molecules through the Boltzmann factor:

$$N_4 = N_T \frac{\exp(-\Delta E_4/kT)}{\sum_n \exp(-\Delta E_n/kT)} \qquad (7)$$

where $\Delta E_n = E_n - E_o$

N_T = total number of S_2 molecules

n = number of vibrational levels in the ground electronic state

For calibration purposes, N_T can be calculated from the amount of solid sulfur placed in the sample tube and the percentage that exists as S_2 at 600°C (discussed more fully at the end of the theory section).

On a macroscopic level, the gas within the sample tube is in overall thermal equilibrium when the temperature stabilizes near 600°C. There are no temperature or pressure gradients since the tube is heated uniformly and completely sealed. The diffusion term $D_f \nabla^2 N_2(t)$ will be approximately zero under these circumstances, and can also be neglected.

From these assumptions based on thermal equilibrium, Equation (5) can now be simplified. Letting N_4 equal a constant and dropping the $B_{24}\rho(\nu)N_2(t)$ and $D_f \nabla^2 N_2(t)$ terms results in:

$$\frac{dN_2(t)}{dt} = B_{42}\rho(\nu)N_4 - (A_{23} + A_2 + Q_2)N_2(t) \qquad (8)$$

or rearranging

$$\frac{dN_2(t)}{dt} + (A_{23} + A_2 + Q_2)N_2(t) = B_{42}\rho(\nu)N_4 \qquad (9)$$

Equation (9) is a first order linear differential equation that can readily be solved.

Solution to the Rate Equation

In solving Equation (9) for $N_2(t)$, the physical events must first be examined to ensure that the mathematical solution accurately describes real phenomena. Two distinct events occur with time in this experiment. First, with the laser pulse on, the population $N_2(t)$ increases due to stimulated absorption from the $v'' = 4$ level. After the laser pulse ends, $N_2(t)$ decreases exponentially with an effective lifetime τ_{eff} due to spontaneous emission and quenching. Once the laser pulse has ended, $B_{42}\rho(\nu)N_4$ vanishes since $\rho(\nu) = 0$. This situation is shown in Figure 5 on the next page, where t_o represents the laser pulse width (10 nsec). Thus, to completely solve Equation (9), two solutions are required. The first is valid during the laser pulse while time varies from $t = 0$ to $t = t_o$. By applying appropriate boundary conditions, this solution to Equation (9) becomes

$$N_2(t) = \tau_{eff}B_{42}\rho(\nu)N_4\,[1 - \exp(-t/\tau_{eff})] \qquad (10)$$

for $0 \le t < t_o$

where $\tau_{eff} = (A_{23} + A_2 + Q_2)^{-1}$

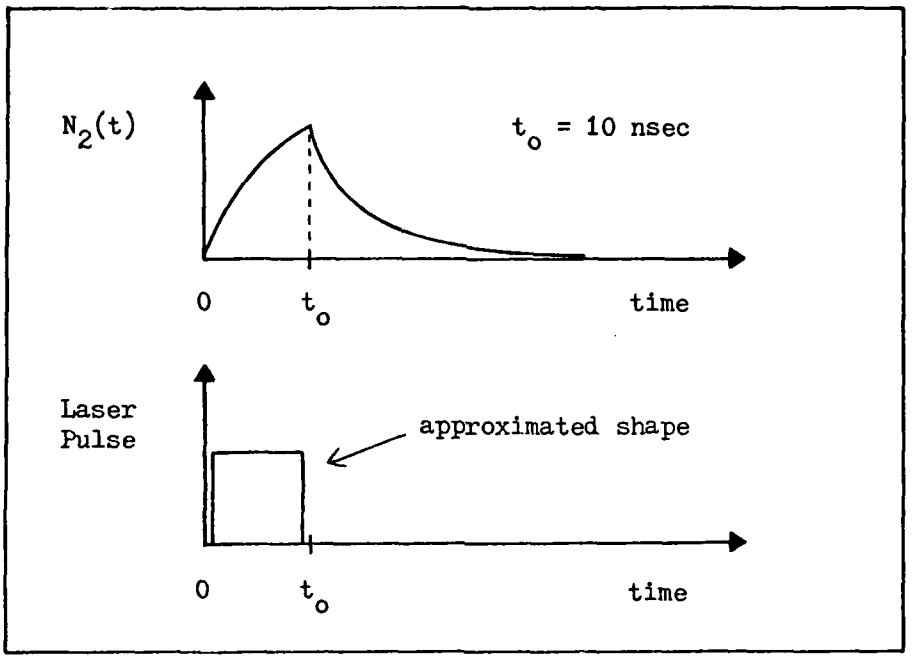

Figure 5. Variation of $N_2(t)$ with Time

The second solution applies after the laser pulse has stopped and $B_{42}\rho(\nu)N_4 = 0$. This solution becomes

$$N_2(t) = \tau_{eff} B_{42}\rho(\nu)N_4 \left[\exp(t_o/\tau_{eff}) - 1\right] \exp(-t/\tau_{eff}) \qquad (11)$$

$$\text{for} \qquad t \geq t_o$$

Since N_4 and N_T are related by the Boltzmann factor, $N_2(t)$ can be solved for as a function of N_T by substituting Equation (7) into Equations (10) and (11).

Observed Fluorescence Intensity

The final step in this analysis relates the S_2 fluorescence intensity to N_T through the method described above. The functional

relationship can then be rearranged to give the desired result, N_T as a function of observed fluorescence. Fluorescence intensity is directly proportional to the upper level number density by the equation

$$I_f(t) = h\nu A_{23} N_2(t) V\Omega/4\pi \qquad (12)$$

where $I_f(t)$ = the observed fluorescence intensity (watts)

ν = the observed transition frequency (Hz)

V = the observation volume (m^3)

Ω = the collection optics solid angle (sr)

Observed fluorescence can also be related to the boxcar output in volts by the formula

$$I_{fb}(t) = K_1 I_f(t) = K_1 [\, h\nu A_{23} N_2(t) V\Omega/4\pi \,] \qquad (13)$$

where K_1 is a parameter with units of volts/watt that represents effects of the spectrometer, PMT, and boxcar. Since $I_f(t)$ is proportional to $N_2(t)$, the observed fluorescence will exhibit the same time dependence as $N_2(t)$ does shown in Figure 5. The total fluorescence signal will also be a combination of two functions, one for each region in time.

In addition to this consideration, the equations for $I_f(t)$ must be further modified because the boxcar integrates the observed fluorescence over the aperture time. The boxcar output is then given by the equation:

$$I_{fb} = \int_{o}^{A_t} I_{fb}(t)dt = K_1 \int_{o}^{A_t} I_f(t)dt \qquad (14)$$

where $I_{fb}(t) = K_1 I_f(t)$ from Equation (13) and A_t equals the aperture time set on the boxcar. The time dependence of $N_2(t)$ necessitates two integrals, one for each region of time

$$I_{fb} = K_1 \int_{o}^{t_o} I_f(t)dt + K_1 \int_{t_o}^{A_t} I_f(t)dt \qquad (15)$$

where the condition $A_t > t_o$ has been assumed. By substituting the expressions for $I_f(t)$ and $N_2(t)$ into Equation (15), carrying out the integration, and combining terms, the intermediate step is obtained

$$I_{fb} = \frac{K_1 h\nu A_{23} V\Omega}{4\pi} \tau_{eff}^2 B_{42} \rho(\nu) N_4 C_t \qquad (16)$$

where $C_t = \{t_o/\tau_{eff} + \exp(-A_t/\tau_{eff}) - \exp[(t_o - A_t)/\tau_{eff}]\}$

Equation (7) can now be substituted into Equation (16) to write N_T in place of N_4. Upon rearranging terms, the desired result is achieved:

$$N_T = \frac{4\pi \sum_n \exp(-\Delta E_n/kT)}{K_1 h\nu A_{23} V \Omega \tau_{eff}^2 B_{42} \rho(\nu) C_t \exp(-\Delta E_4/kT)} I_{fb} \qquad (17)$$

where Table I on the next page summarizes the nature of each parameter. Equation (17) is the theoretical relationship that gives the total S_2 number density as a function of the observed fluorescence intensity from the $v' = 2$, $v'' = 3$ transition, based on the assumptions made in

Table I

Summary of Parameters in Equation (17)

Constants	Sulfur Data	Determined from Set-up and Equipment	Measured during Experiment
4π h	A_{23} B_{24}	V Ω	τ_{eff} I_{fb}
k K_1	ΔE_n ΔE_4	T t_o	C_t
	ν	A_t $\rho(\nu)$	

this derivation and analysis.

Experimental Considerations

Once the equipment is set up for an experiment, all parameters in Equation (17) become constants except τ_{eff}, $\rho(\nu)$, C_t, and I_{fb}. τ_{eff} and C_t vary with the amount of S_2 present, while $\rho(\nu)$ varies because the laser output power changes slightly from run to run. Based on this, Equation (17) can be reduced to the more basic form

$$N_T = \frac{K}{\tau_{eff}^2 \rho(\nu) C_t} I_{fb} \qquad (18)$$

where K is a constant that combines the effects of all other parameters. Using precalibrated sample cells with a known S_2 number density N_T,

Equation (18) can be solved for K by measuring τ_{eff}, $\rho(\nu)$, C_t and I_{fb}. This value of K can then be used to determine N_T under other conditions by measuring the fluorescence intensity I_{fb} (along with τ_{eff}, $\rho(\nu)$, and C_t). If precalibrated cells are not available, N_T can be calculated from the amount of solid sulfur placed in the sample tube, and the percentage of molecules which exist as S_2 at the operating conditions examined (discussed more fully in the next paragraphs). This calculated N_T can then be used to determine K and other number densities as outlined above.

Sulfur Vapor Composition

When precalibrated sample cells are not available, S_2 number densities must be calculated from known chemical data. This task is complicated by the complex and often not understood behavior of sulfur, particularly its molecular composition while in the vapor phase. As a vapor, sulfur is known to exist in various combinations of S_8, S_7, S_6, S_5, S_4, S_3, and S_2 molecules, the concentration of each depending on the temperature and pressure. Near temperatures of 160°C, the vapor consists primarily of S_8 chains, formed from S_8 molecular rings that exist in the liquid sulfur (Ref 19:95). As the temperature is raised to 600°C, the S_8 chains thermally dissociate to produce S_2 molecules. Since the boiling point of sulfur occurs at 445°C, low pressures are needed to completely vaporize the solid sulfur. Figure 6 on the following page gives a plot of total sulfur vapor pressure versus temperature.

To provide the reference mentioned above, S_2 number densities can be calculated from the amount of solid sulfur placed in the sample tube. However, in converting from grams of sulfur to molecules of S_2,

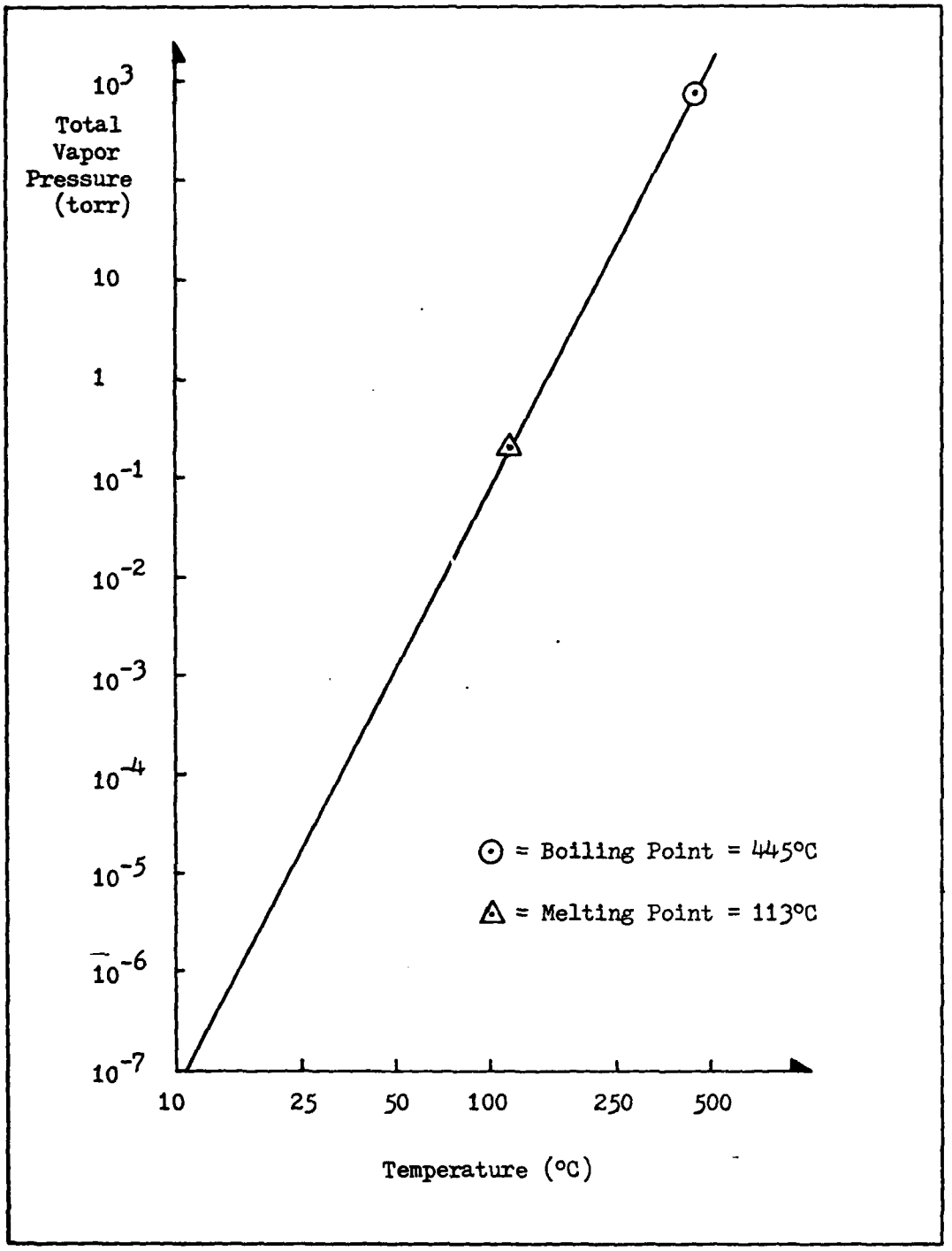

Figure 6. Sulfur Vapor Pressure versus Temperature (Ref 14:4-300)

there is still some uncertainty as to what percentage of the vapor actually exists as S_2 near 600°C. Several researchers have used gas-phase equilibrium constants to calculate that over 98% is S_2 near this temperature (Ref 1:822). If this percentage is accepted, other sulfur species near 600°C can be ignored, and the overall chemical equilibrium approximated by

$$S \rightleftarrows (.5)S_2 \tag{19}$$

Theoretical S_2 number densities can then be calculated from Equation (19) based on the sample's weight in grams.

On the other hand, Braune and his co-workers experimentally determined that only 78% of the sulfur vapor exists as S_2 near 600°C, and have reported spectroscopic evidence for several other molecules at this temperature (Refs 6:33-37 and 19:149-150). To calculate the amount of S_2 formed with Braune's results, Dalton's partial pressure law can be used in the following form (Ref 23:130):

$$\frac{P_i}{P_T} = \frac{n_i}{n_T} \tag{20}$$

where P_i = partial pressure of each species

P_T = total pressure of sample

n_i = number of moles of each species

n_T = total number of moles in sample

The quantity n_i/n_T gives the proportion of each molecule present in the overall chemical reaction. Assuming as Braune did that S_2, S_4,

S_6, and S_8 are all present at 600°C, his data can be used to modify Equation (19). The new equilibrium can be written

$$S \rightleftarrows (.337)S_2 + (.065)S_4 + (.010)S_6 + (.0004)S_8 \qquad (21)$$

based on measurements made at a temperature of 600°C and total pressure of 92.5 torr (Ref 19:150). Since the molecular proportions in Equation (21) are pressure-dependent, the theoretical conversion of Equation (19) was used to calculate total S_2 number densities used later in the report. This was done to provide a standard reference throughout the results section.

IV. Equipment

The equipment used in this thesis is discussed under the following topics: (1) laser, (2) oven, (3) sample tubes, (4) optics through photomultiplier tube, and (5) electronics. The overall set-up is shown in Figure 7 on the following page.

Laser

The laser used for this experiment was a molectron Model UV1000 pulsed nitrogen (N_2) laser operating at 3371 Å. Pulse rates of 5, 10, 15, 20, 25, 30, 40, and 50 Hz are available, with the requirement that N_2 gas flow be adjusted at each setting for optimum power output. For this research, pulse rates of 10 or 20 Hz were generally used. The Molectron laser produces one megawatt peak power with a pulse width of approximately 10 nsec. Since the laser output at 3371 Å so closely matched the $v' = 2$, $v'' = 4$ transition in S_2 at 3369.6 Å, a tunable dye laser was not needed to pump the $v' = 2$ band.

Oven

The oven used in this experiment was locally fabricated in the laboratory and measures 22 cm wide, 45 cm long, and 28 cm tall. It is constructed out of sheet metal and lined with fiber-frax insulation. The oven is heated electrically with nichrome wire filaments strung along the inside walls. Oven temperature is regulated by a Fenwal Model 524 temperature controller, and monitored with an Omega Engineering Model 199 digital temperature gauge and Type K thermocouple. The oven has 38 mm diameter circular quartz windows on both ends to allow the laser beam to pass through, and a 32 mm diameter circular quartz window on one side to view the fluorescence signal. Quartz windows are

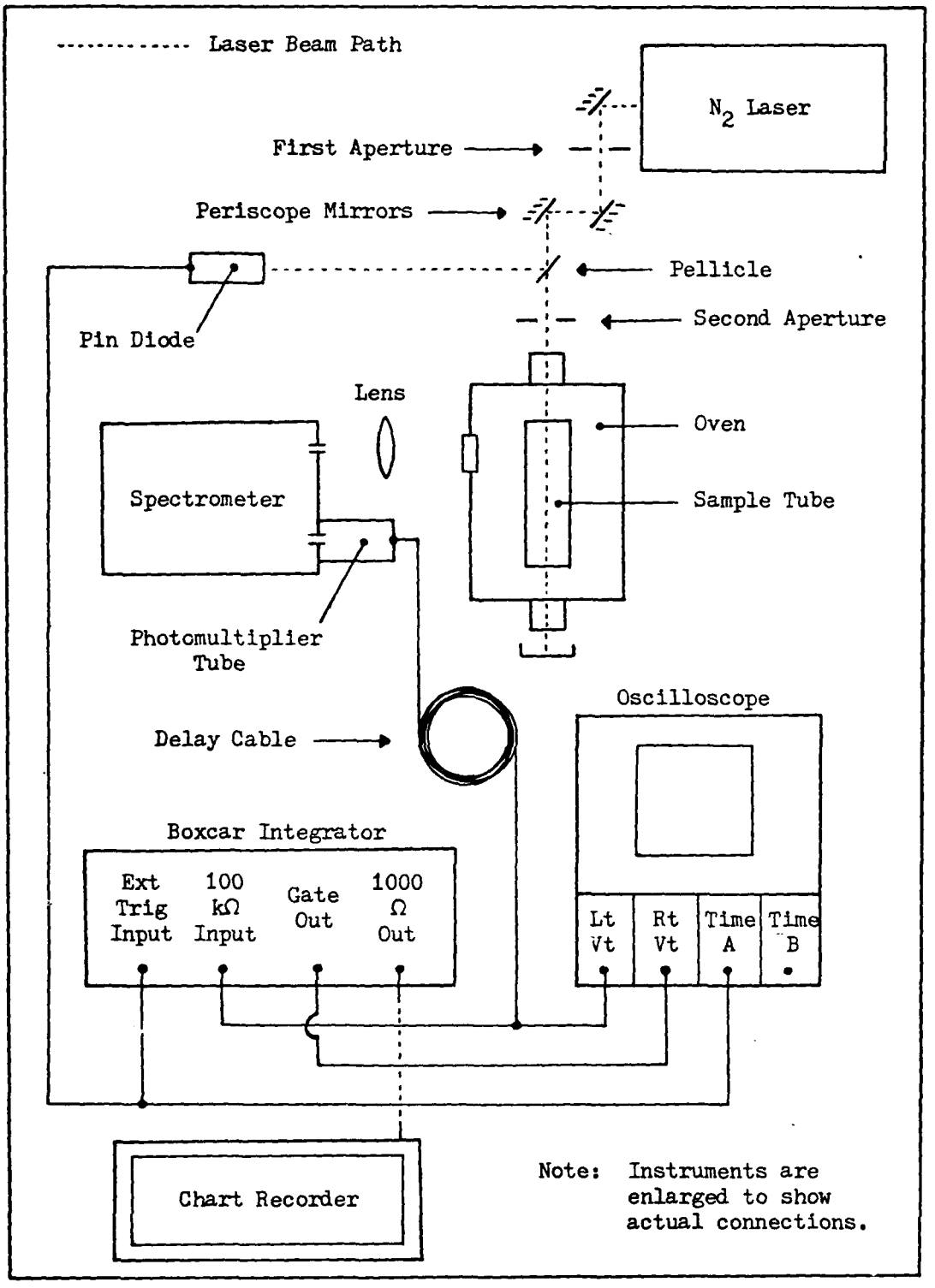

Figure 7. Experimental Set-up

necessary for high temperature operation and maximum transmission of the UV beam. The sample tube is placed into the oven through an opening in the top, and rests on a "v" shaped cradle inside.

Sample Tubes

The sample tubes are also fabricated in the laboratory and vary in size from 13 to 38 cm in length and from 2 to 4 cm in diameter. They are constructed from quartz tubing and windows, and are evacuated to approximately 10^{-7} torr. Pressures at desired operating temperatures are controlled by placing a known amount of solid sulfur inside the tubes before they are sealed off. The sulfur used in this experiment was manufactured by Eagle-Picher of Oklahoma with a 98% purity.

Optics Through Photomultiplier Tube

The laser output beam first passes through a 12 mm diameter circular aperture to limit its extent and provide a cleaner profile for reflection off the periscope mirrors. A pellicle beam splitter reflects 15% of the beam toward the PIN diode, allowing the rest to pass through the oven and sample tube. The beam entering the oven passes through a 5 mm diameter circular aperture to further limit its extent and provide an intense cross-section without focusing.

The fluorescence signal is collected at right angles to the laser beam by a 9 cm diameter lens with a 20 cm focal length. The emitted signal is focused into the entrance slit of a Jarrell-Ash Model 82-000 half-meter Ebert scanning spectrometer. This spectrometer contains a 52 mm by 52 mm grating ruled at 1180 groves/mm and blazed for 4000 Å in the first order. The reciprocal linear dispersion at the exit slit is 16 Å/mm under these conditions.

The output of the spectrometer passes into an Emitronics (EMI) Model 9816B photomultiplier tube (PMT) for detection. This tube contains a 14 stage linear diode chain and provides an S-20 response, covering the approximate range of 3000 to 8000 Å. Peak response occurs at 4000 Å with an absolute sensitivity of 70 mA/watt and quantum efficiency of 23%. The PMT is run at 1900 volts, powered by a Hewlett-Packard Model 6516A DC power supply.

Electronics

The output from the PMT passes through 150 ft of delay cable for timing purposes, then is sent to the Princeton Applied Research (PAR) Model 160 boxcar integrator. Since the S_2 fluorescence signals are usually on the order of the PMT dark current noise in intensity, a method is needed to distinguish these signals from background noise. The boxcar uses a sampling and averaging technique to average out the noise over a large number of repetitions. The signal-to-noise ratio is greatly improved, and the output of the boxcar asymptotically approaches the average value of the fluorescence signal over the time period examined. The boxcar integrator can also scan across the input signal, reproducing the entire waveform without noise.

For examining individual S_2 transitions, the boxcar is run in the sample and hold mode, triggered externally by the PIN diode. Timing between the boxcar sampling gate (aperture), PMT signal, and trigger pulse is monitored during the experiment on an oscilloscope. The high and normal resolution time constants are selected to provide a visible but stable needle deflection on the boxcar output meter. Since events in this experiment occured with nanosecond times, the time base was set at 2 μsec (shortest available), while the aperture was 30 nsec wide.

To record the S_2 spectrum, the boxcar output was sent to a Hewlett-Packard Model 7132A chart recorder.

To monitor the timing mentioned above, a Tektronix Model 7104 oscilloscope was used. The 7104 scope was also employed during the experiment to troubleshoot, display and record the fluorescence signal. Tektronix Model 7A29 amplifiers and Models 7B15/7B10 time bases comprised the plug-in units for the scope, giving it the response characteristics needed for this research. A Tektronix Model C-50/C-70 oscilloscope camera was used to photograph the displayed signal.

Laser output power was checked during the experiment with two different instruments. To measure average power, a Scientech Model 362 power/energy meter and Model 3600 detector were used. Peak power can then be calculated from the pulse rate, pulse width, and measured average power. To calculate actual average power per pulse, the Scientech measured power was first divided by the pulse rate, then divided by the pulse width.

For sensitive measurements beyond the Scientech's capability, an Eppley laboratory thermopile and Keithley Instruments Model 148 nanovoltmeter were used. The nanovoltmeter reading was converted to average power through a watts per volt conversion factor calculated at 3371 Å. Power loss through each optical component was also measured with these instruments. Laser power within the sample tube could then be calculated from reference powers measured at the beginning and end of each data run.

V. Procedure

In this section, the experimental procedure is discussed, organized under the following main topics: (1) broad spectrum, (2) long-lived states, (3) fluorescence intensity measurements, (4) fluorescence lifetime measurements, and (5) problem areas.

Broad Spectrum

The first step in this experiment was to detect the S_2 fluorescence. Equipment was set up as shown in Figure 7 in the preceeding section, the PIN diode used to trigger both the boxcar and oscilloscope. The boxcar was run in the sample and hold mode, with a time base of 2 μsec, high resolution time constant of 3 nsec, normal resolution time constant of .3 msec, aperture time of 30 nsec, and stretch time of 30 μsec. The laser pulse was used to check for proper triggering and optimum signal retention, while scattered radiation from the laser was detected to estimate boxcar input sensitivities and chart recorder settings.

The spectrometer was initially scanned from 3300 to 5000 Å at 125 Å/min. The entrance slit was set at 200 μ, while the exit slit was opened to 600 μ. The entrance and exit slits were both 1 cm in height. Scans during this portion of the experiment were always made in pairs. The first run took place at room temperature (21°C) in order to record laser scatter, background signals, and PMT dark current noise. At this temperature, sulfur is still in solid form since its melting point does not occur until 113°C (Ref 19:95). For the second run, the oven was heated to approximately 600°C. This was necessary to vaporize the sulfur and thermally dissociate the S_8

chains, predominant at low temperatures, into S_2 molecules. Once the spectrum was obtained, it was calibrated with N_2 laser scatter and a mercury reference run. Fluorescence peaks were identified by comparing the observed values with Tables III-V in Peterson and Schlie's work (Ref 21:1559-1561).

Long-lived States

With the S_2 spectrum identified, scans were made to determine which transitions were long-lived. Settings were the same as in the previous section, the spectrometer again being run at 125 Å/min. After each scan, the initial delay on the boxcar was increased by 1% (20 nsec on time base). This method provided a means of filtering out the short-lived states, leaving only those whose fluorescence lifetimes were considerably longer.

Fluorescence Intensity Measurements

After identifying the S_2 spectrum and determining which transitions were long-lived, prominent lines were further examined to determine their suitability for fluorescence intensity measurements. The $v' = 2$, $v'' = \bar{3}$ transition at 3290.7 Å was chosen for its high Franck-Condon factor (.113), strong emission intensity, and relatively long lifetime. The spectrometer was set to this wavelength, and data collected with all three sample tubes.

S_2 fluorescence intensity versus temperature measurements were made by gradually heating the oven from room temperature to 600°C. This process took almost two hours, allowing ample time to take intensity readings at selected temperatures. The entrance slit was kept at 200 μ, while the exit slit was opened to 1500 μ to account for the

spectrometer's dispersion (the bandwidth of the input fluorescence signal was approximately 25 Å). The boxcar normal resolution time constant was increased to 3 msec to hold the signal longer and provide better noise filtering. With these settings and the length of time required to heat the oven, the boxcar output became very steady.

Once the oven reached equilibrium near 600°C, fluorescence intensity versus laser power readings were taken. This was accomplished by placing neutral density filters in the path of the laser beam going into the oven and sample tube. The boxcar output was then recorded as different combinations of filters were used. Each filter was specifically calibrated at 3371 Å by measuring its attenuation of a reference beam with the Scientech power meter.

Fluorescence Lifetime Measurements

S_2 fluorescence lifetime measurements at specific temperatures and pressures were made directly from the oscilloscope display using the Tektronix camera. Single sweeps were photographed to examine individual pulse shape, while several sweeps exposed on the same photograph provided an average profile. Equipment settings were the same as those used for fluorescence intensity measurements.

Problem Areas

Several problems occured during the experiment that were severe enough to cause work stoppage. Most were corrected and overcome in a short time, but some are system-inherent and ones future researchers should be aware of. These problems are discussed under the topics: (a) laser, (b) triggering/timing, and (c) boxcar.

Laser. Three major problems were experienced using the Molectron

laser. The first occured when a large power supply transformer for the thyratron cathode filament burned out, disabling the thyratron and laser. Troubleshooting produced a shorted wire near one of the transformer's terminals. This wire and the nearby windings were repaired by laboratory machinists, and the transformer returned to service.

A second problem arose from the large amounts of ozone produced by the laser, especially at higher repetition rates. Ozone is dangerous because of its toxic and explosive properties. During the experiment, ozone rapidly collected in the laboratory since the exhaust system was unable to keep up with the high formation rate. Concentrations were high enough to detect by smell, the odor threshold of ozone being 0.1-0.015 ppm by volume of air for the normal person (Ref 5:76). The recommended threshold limit value for repeated ozone exposures during an 8-hour working day is 0.1 ppm, while symptoms of acute ozone toxicity appear at concentrations of about 1 ppm. An extra exhaust pipe had to be placed near one end of the laser to properly vent the ozone outside.

The final laser problem encountered during this experiment was the slight decrease in laser output power over long data-gathering sessions. The operating pressure also tended to increase by several torr. Both of these phenomena are inherent in lengthy operation of the laser, and necessitated "before and after" laser power measurements. The decrease in average power was found to be anywhere from 0.5 to 4.0 mW as measured on the Scientech power meter (.7 to 6% reduction in actual power). Slight output power variation from pulse to pulse was also noticed, and is discussed in the next paragraphs.

Triggering/Timing. Another problem that developed during long data runs was that of triggering and timing stability. Slight fluctuations

in laser output power from pulse to pulse and over time caused corresponding fluctuations in the PIN diode output. As a result, PIN trigger pulses sent to the boxcar were not always identical in shape and amplitude. This variation in waveform caused boxcar circuitry to trigger the time base ramp at different points in time relative to the PMT signal. Figure 8 on the next page illustrates the relationship between boxcar triggering, input PIN pulses, and the start of the time base circuitry. Since the sampling gate opens at a fixed interval after the time base ramp starts, this variation in triggering caused the sampling gate to sometimes miss the fluorescence signal. The boxcar output voltage fluctuated greatly under these conditions, depending on whether the sampling gate was averaging over the PMT signal or dark current noise. The start of the time base ramp varied from 20 to 100 nsec relative to the PMT signal. To minimize this problem, a PIN diode with a large output (3 V) was used. The boxcar was triggered off the decay side of the PIN waveform, which lasted for approximately 60 nsec. This change provided more consistent trigger points and compensated somewhat for the laser output power fluctuations. The time base ramp starting point varied only slightly (< 10 nsec) under these conditions.

Boxcar. The boxcar used in this experiment is a versatile instrument, but requires a detailed understanding to set it up properly. Operation is further complicated when using the high resolution mode, as needed in this research. A "pitfalls" section included in the manual helps one choose the right settings, but some of the more subtle problems are worth discussing. First, there is an unavoidable delay of 150 nsec between triggering of the boxcar and start of the time base

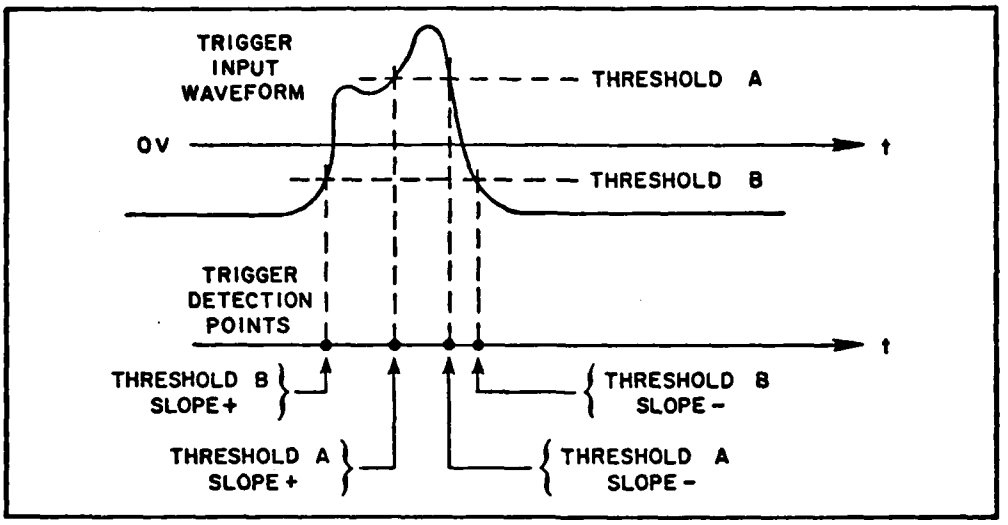

Figure 8. Boxcar Triggering Relationships (Ref 17:III-6)

ramp. This delay is due to internal circuitry, and necessitated placing 150 feet of delay cable in the PMT output to delay the fluorescence signal by an extra 150 nsec. In addition, the initial delay dial should not be set less than 5%. This value is the minimum allowed to ensure proper time base generation. When choosing the time constants for an experiment, the observed time constant (OTC) must be calculated using formulas given in the manual. This result is needed since it takes boxcar capacitors five times the OTC in real time to charge up their maximum value (Ref 17:III-14). If the event is not examined long enough according to this criterion, the boxcar output will show a lower-than-actual value. Finally, the retention control must be optimized once all other settings are selected. This control enables the boxcar to hold the signal better between each triggering and sampling event, and to reduce the signal bleed-off due to capacitor discharge.

VI. Results and Discussion

The experimental results are presented in this section, along with calculations based on the rate equation model. The data and analysis is discussed under the topics of: (1) broad spectrum, (2) fluorescence intensity measurements, (3) fluorescence lifetime measurements, (4) number density calculations, and (5) error analysis.

Broad Spectrum

The broad S_2 spectrum obtained in this experiment is shown in Figure 9 on the following page. All lines belong to the $v' = 2$ band since the laser pumped the $v' = 2$, $v'' = 4$ transition. Table II on page 44 summarizes the important data from this spectrum. The relative intensities of each line closely follow the Franck-Condon factors for these transitions, related through the equation (Refs 1: 821 and 16:200):

$$I_{v'v''} = \frac{64\pi^4\nu^4}{3c^2}(\bar{R}_e)^2 N_{v'} q_{v'v''} \qquad (22)$$

where $I_{v'v''}$ = the observed fluorescence intensity

$\bar{R}_e$ = the average electronic transition moment

$N_{v'}$ = the excited state population

$q_{v'v''}$ = the Franck-Condon factor for the v'-v" transition

Equation (22) neglects rotational effects that would have to be included under a more detailed analysis. To a first order approximation,

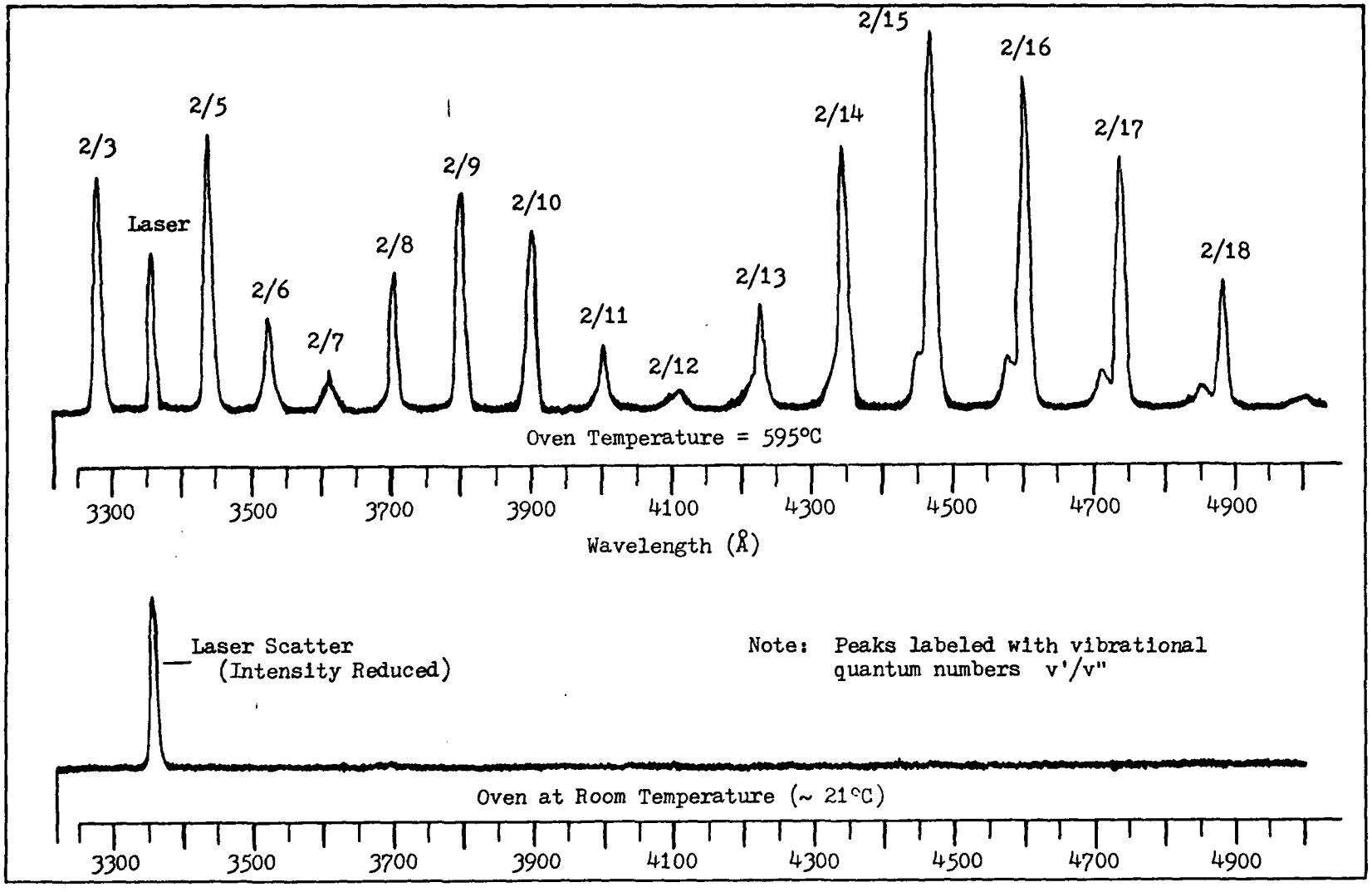

Figure 9. Broad S_2 Spectrum

Table II

Data from Broad S_2 Spectrum

Observed Wavelength (Å)	Actual Wavelength (Å) (Ref 21)	Franck-Condon Factor $q_{v'v''}$ (Ref 21)	Vibrational Quan. Numbers v'/v"
3294	3290.7	.113	2/3
3452	3451.0	.077	2/5
3539	3534.3	.020	2/6
3624	3622.0	.005	2/7
3718	3713.9	.041	2/8
3812	3810.8	.073	2/9
3912	3909.6	.060	2/10
4016	4012.5	.016	2/11
4125	4120.8	.002	2/12
4241	4235.8	.022	2/13
4360	4355.0	.065	2/14
4484	4478.8	.072	2/15
4615	4610.0	.102	2/16
4754	4747.6	.076	2/17
4900	4892.4	.046	2/18

$N_{v'}$ can be replaced by $N_{J,v}$ from Equation (1) in the theory section to estimate changes produced by the rotational distribution.

Fluorescence Intensity Measurements

Fluorescence intensity versus temperature measurements for the $v' = 2$, $v'' = 3$ transition are plotted in Figure 10 on the next page. The first signs of S_2 occur between 350-400°C, which agrees well with previous research. In an equilibrium composition of sulfur vapor, S_2 starts to form near 240°C, and reaches 1% concentrations around 350°C. However, as the temperature is increased, the results in Figure 10 show a more rapid increase in S_2 formation than expected. Near 475°C, the observed fluorescence intensity had already reached from 25 to 68% of its maximum value, depending on the pressure. Meyer's data shows that only 3% of the sulfur vapor is S_2 at this temperature (Ref 19:149). This acceleration in S_2 formation may result from the low pressures used in this research. Near 475°C, the partial pressure of S_2 in the sample tubes was roughly .1-6 torr.

Quenching is evident since the observed fluorescence intensity reached a larger percentage of its peak value at lower pressures (for the same temperature). At a constant temperature, quenching can be approximated by the equation (Ref 29:11)

$$Q_2 \approx q_r P \qquad (23)$$

where q_r is the quenching rate constant and P the pressure. Thus, quenching effects would increase as the pressure increases.

The decreases in intensity above 560-570°C shown in Figure 10 were investigated further and found to be real phenomena. To explain

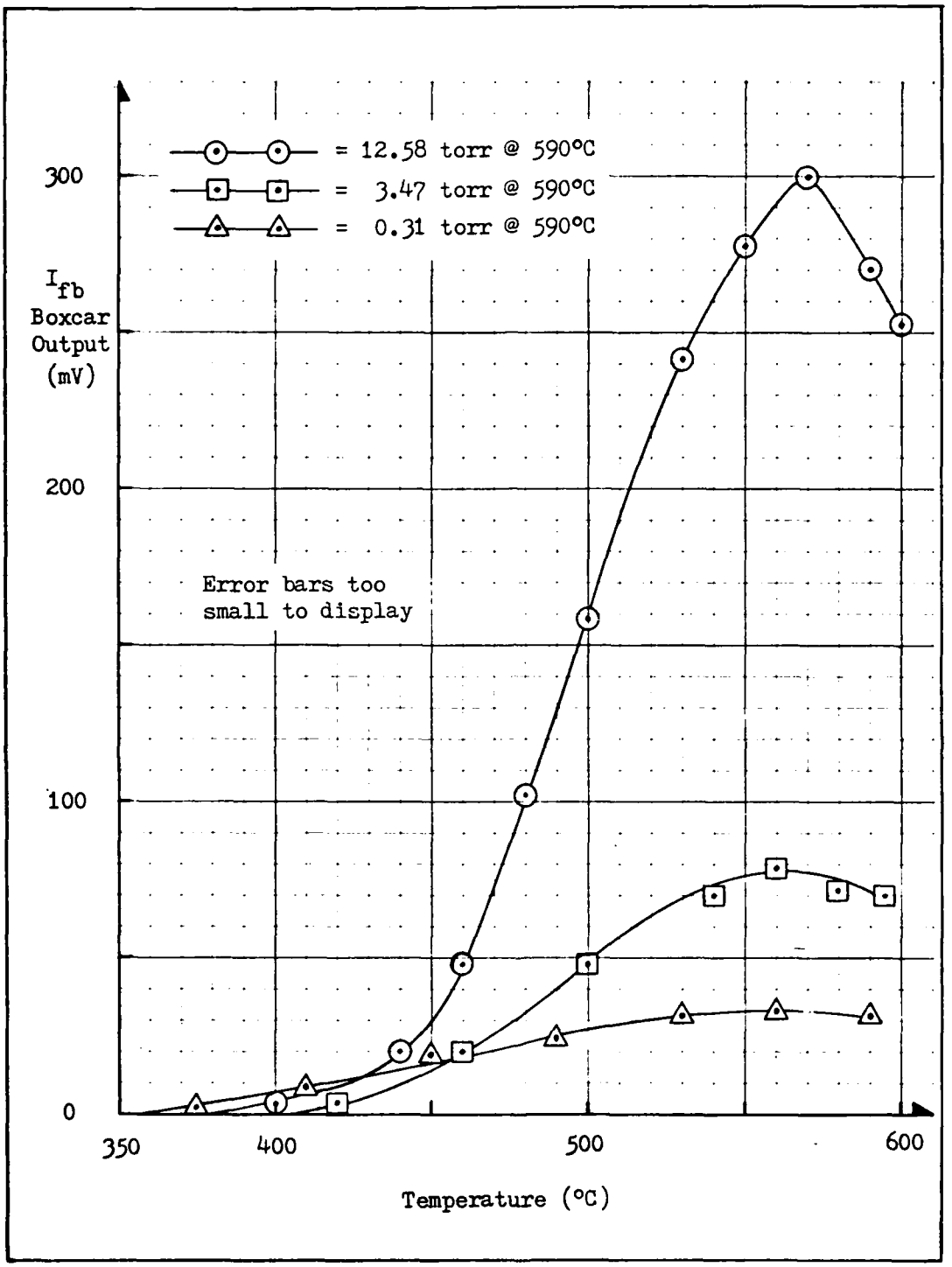

Figure 10. S_2 Fluorescence Intensity versus Temperature

this occurrence, four possible mechanisms are considered. First, the total quenching rate Q_2 may be increasing due to the increasing pressure, as described in Equation (23). This would cause a greater depopulation of the $v' = 2$ level through nonradiative means, leaving fewer $N_2(t)$ molecules to contribute to the observed fluorescence. A second possibility results from the fact that the concentration of each sulfur molecule (S_8, S_7, S_6, etc.) depends on the temperature and pressure of the vapor. Thus, as the temperature and pressure change, so do the equilibrium proportions and mole fractions calculated for Equation (21) in the theory section. In this case, since the intensity is decreasing, S_2 molecules may be combining to form other molecules and lower the S_2 concentration. Radiation trapping is a third process which may contribute to the intensity reduction at higher temperatures. Radiation trapping occurs when there is a high probability that an emitted photon will be immediately re-absorbed (Ref 25:386). This process increases as both the number density of molecules and their thermal motion increases. In addition, once the radiation is absorbed, it may be re-emitted at different wavelengths and in different directions. Therefore, the fluorescence intensity at the observed wavelength will decrease as radiation trapping increases. Finally, the thermal distribution of rotational levels may also be a factor under these conditions. As shown in Figure 4 in the theory section, this distribution can greatly affect the intensity of a vibrational-rotational line. As the temperature increases, the reduction in intensity may result from the decrease in population of the initial rotational levels.

Fluorescence intensity versus laser power measurements are shown

in Figure 11 on page 49, and exhibit the linear relationship referred to in the theory. From this plot, it is clear that even partial saturation of the $v' = 2$, $v'' = 4$ transition did not occur. This result formed the basis of the decision not to use saturation approximations in solving the rate equation for $N_2(t)$.

Fluorescence Lifetime Measurements

After the laser pulse was turned off, effective lifetimes for the $v' = 2$, $v'' = 3$ transition were determined by measuring the time required for the intensity to drop to 1/e of its initial value (e = the natural logarithm constant). These measurements were performed on photographs of the fluorescence signal taken from the oscilloscope display. Since the radiative lifetime τ_{rad} for this transition is equal to the inverse of the A_{23} coefficient, Equation (10) can be used to relate the effective lifetime τ_{eff} to τ_{rad} and quenching. This relationship becomes

$$\tau_{eff} = (1/\tau_{rad} + A_2 + Q_2)^{-1} \qquad (24)$$

Assuming that A_2 stays relatively constant, when quenching effects are significant, Q_2 becomes large and τ_{eff} decreases. If quenching is approximated with a linear function of pressure as in Equation (23), then τ_{eff} should decrease as the operating pressure increases.

In this experiment, exactly the opposite behavior was observed. As seen on page 50, τ_{eff} increased as the pressure increased. In addition to quenching effects, this deviation is probably caused by radiation trapping. Radiation trapping causes the observed lifetime to be much longer than the true effective lifetime if this process were

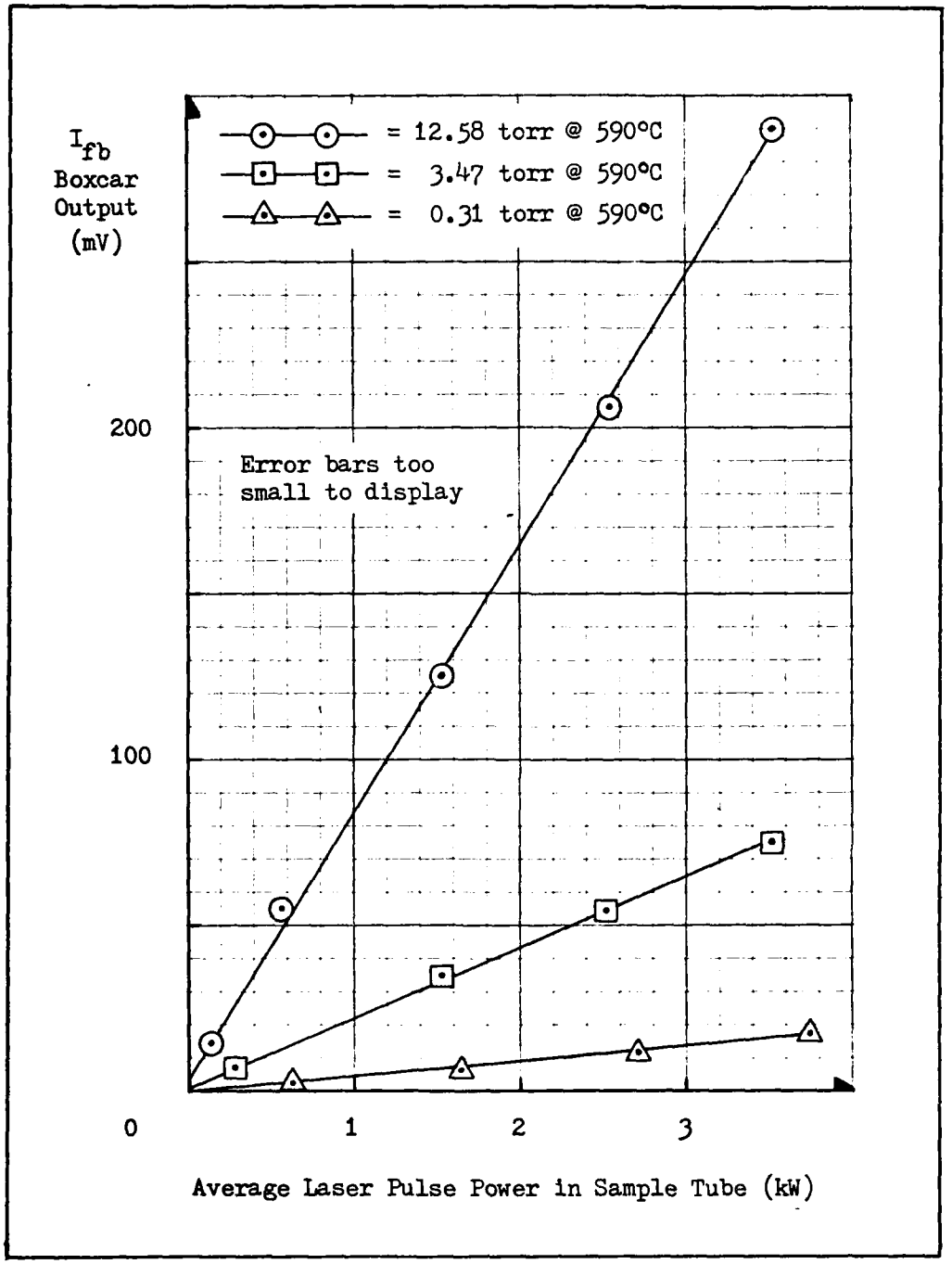

Figure 11. S_2 Fluorescence Intensity versus Laser Power at 590°C

not occuring (Ref 25:386). From photographs of the fluorescence signal, the following lifetimes were determined:

Pressure at 590°C	Effective Lifetime
0.31 torr	8 ± 3 nsec
3.47 torr	14 ± 3 nsec
12.58 torr	20 ± 2 nsec

Using a phase shift method, Smith has calculated an average radiative lifetime of 16.9 ± 3.5 nsec for transitions within the $v' = 2$ band (Ref 26:1194). The boxcar integrator was not used to measure fluorescence lifetimes since it introduces large time distortion while scanning in the high resolution mode. This occurs because the shortest aperture time available is 5 nsec.

Number Density Calculations

S_2 number densities versus pressure at 590°C are plotted in Figure 12 on the following page. The reference amounts were calculated assuming 98% S_2 near 600°C. Recalling Equation (18) from the theory section, the number density is related to the observed fluorescence intensity by the formula

$$N_T = \frac{K}{\tau_{eff}^2 \rho(\nu) C_t} I_{fb} \qquad (18)$$

where I_{fb} is the boxcar output voltage. The sample tube with a pressure of 3.47 torr at 590°C was used to calibrate the system and solve Equation (18) for K knowing N_T. Table III on page 52 summarizes this data.

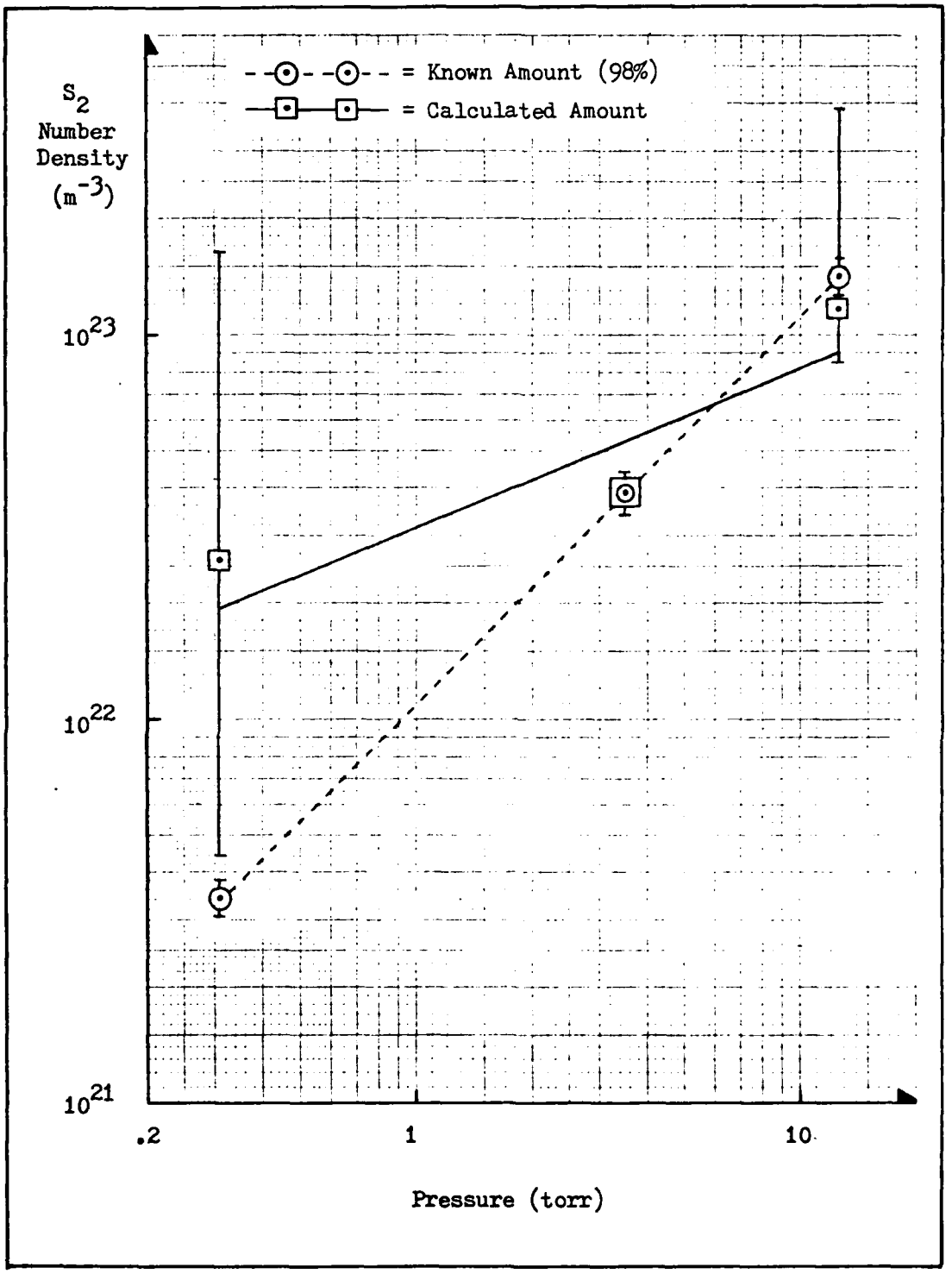

Figure 12. S_2 Number Density versus Pressure at 590°C

Table III

Data from S_2 Number Density versus Pressure

Pressure (torr)	Known Number Density (98% S_2) (m^{-3})	Calculated Number Density * (m^{-3})
0.31	$3.4 \pm .3 \times 10^{21}$	$2.6 \pm 8.0 \times 10^{22}$
3.47	$3.9 \pm .4 \times 10^{22}$	--
12.58	$1.4 \pm .1 \times 10^{23}$	$1.2 \pm 2.7 \times 10^{23}$
* $K = 1.8 \pm 2.5 \times 10^{-2}$ from 3.47 torr pressure as reference		

As shown in Figure 12, there is some disagreement between the theoretical (98%) number densities and those determined from experimental data using Equation (18). The differences are within one order of magnitude, however the low pressure value is undesirable since it is actually larger than the known amount of S_2. If the calculated line is extended, these differences will increase and quickly become greater than two orders of magnitude. Part of this deviation may be caused by the uncertainty in the effective lifetimes measured from the oscilloscope. However, even if the lifetimes are increased to 20 nsec at all pressures, the calculated number densities are still larger than the theoretical values at low pressures.

Error Analysis

Most errors originated from the measurements and data taken during the experiment. For data used from other works where no uncertainties were given, a 10% error was assumed. Errors were propagated using the method of computing average deviations. With this method, absolute errors are added for the operations of addition and subtraction, while relative errors are added for calculations involving multiplication and division (Ref 15:Sec A2, 8-9).

The results obtained in this experiment suggest that the theory may not adequately model the observed transition. If this is true, the theory and derivations must be re-examined. One source of error arises because stimulated emission from the $v' = 2$ level has been neglected. If included, this process would reduce $N_2(t)$ while the laser pulse was on. Keeping the stimulated emission term throughout the derivation would slightly modify Equations (17) and (18). For reasons discussed earlier, the effective lifetime measurements also introduced large uncertainties into these calculations. Besides being difficult to measure from a photograph, the effective lifetimes were affected by the processes of quenching and radiation trapping. The theoretical number density N_T used to calculate K in Equation (18) represents a third source of error in this analysis. This error results from the uncertainty in determining what percentage of the sulfur vapor exists as S_2 at the desired temperature. Overall, the results of this section show that laser induced fluorescence can be used to measure S_2 number densities, but that a more detailed theoretical treatment is needed to improve the accuracy of the model.

VII. Summary, Conclusions, and Recommendations

Summary

This thesis investigated the feasibility of using laser induced fluorescence to measure S_2 number densities in a laboratory environment. The research was prompted by the growing interest in S_2, especially its potential as a tunable, high-power laser medium. A rate equation analysis was performed on transitions within the $B^3\Sigma_u^- - X^3\Sigma_g^-$ system in order to model their energy level interactions. The $v' = 2$, $v'' = 3$ transition at 3290.7 Å was selected for nonresonance fluorescence studies due to its prominence and accessibility. The excitation source for this experiment was a pulsed nitrogen laser operating at 3371 Å. A tunable dye laser was not needed since the laser efficiently pumped the $v' = 2$, $v'' = 4$ S_2 transition at 3369 Å. Investigations included broad spectrum identification, fluorescence intensity versus temperature and laser power measurements, effective lifetime measurements, and total number density calculations. All data was taken near 600°C to ensure that a large percentage of the sulfur vapor was S_2 ($\geq$ 98%). Results were compared with theory to evaluate the rate equation model and laser induced fluorescence technique. Experimentally determined number densities were too large in the low pressure region, but generally within one order of magnitude over the range examined. Aside from the problems discussed in Section V, the equipment worked well and produced repeatable results.

Conclusions

In concept, laser induced fluorescence proved to be a feasible means of measuring S_2 concentrations in a laboratory environment.

Differences between the known and calculated number densities are attributed to the complexity of S_2, quenching and radiation trapping, difficulties in measuring the effective lifetime, and inadequacies in the rate equation model. The accuracy of this analysis could be improved by a more detailed theoretical treatment, especially by incorporating stimulated emission and rotational effects into the derivation. In addition, an improved method of determining the effective lifetime would reduce some of the uncertainty encountered in this experiment.

Recommendations

Based on the results of this experiment, the use of laser induced fluorescence to measure number densities should be studied further. The benefits would include increased knowledge of the molecule studied and refinement of the laser induced fluorescence method, especially in situations where the steady state and saturation approximations cannot be applied. Specific recommendations for future research of the laser induced fluorescence technique include:

1. Perform fluorescence intensity measurements over a wider range of pressures.
2. Develop a more effective way of measuring effective lifetimes, possibly with an advanced model boxcar integrator.
3. Incorporate stimulated emission and rotational effects into the rate equation model to improve its accuracy.
4. Quantitatively estimate the magnitude of quenching and radiation trapping effects, and include these as corrections to the observed fluorescence intensity.

Specific recommendations for future sulfur research include the following:

1. Focus the laser beam to a point in the sample tube in

order to saturate the transition being investigated.

2. Use a tunable dye laser to pump and examine other transitions that might be more amenable to the theory developed.

3. Increase the operating temperature above 600°C or use radio frequency discharges to ensure that a higher and more exact percentage of S_2 is formed.

Bibliography

1. Anderson, William R., David R. Crosley, and John E. Allen, Jr. "Franck-Condon Factors for the B-X System of S_2," Journal of Chemical Physics, 71 (2): 821-829 (July 1979).

2. Banwell, C. N. Fundamentals of Molecular Spectroscopy (Second Edition). London: McGraw-Hill Book Company (UK) Limited, 1972.

3. Baronavski, Andrew P. and J. R. McDonald. "Measurement of C_2 Concentrations in an Oxygen-acetylene Flame: An Application of Saturation Spectroscopy," Journal of Chemical Physics, 66 (7): 3300-3301 (April 1977).

4. Baronavski, A. P. and J. R. McDonald. "Application of Saturation Spectroscopy to the Measurement of C_2, $^3\pi_u$ Concentrations in Oxyacetylene Flames," Applied Optics, 16 (7): 1897-1901 (July 1977).

5. Braker, William, and Allen L. Mossman. Effects of Exposure to Toxic Gases - First Aid and Medical Treatment. East Rutherford, New Jersey: Matheson Gas Products, 1970.

6. Braune, Von H., S. Peter, and V. Neveling. "Die Dissociation des Schwefeldampfes (The Dissociation of Sulfur Vapor)," Zeitschrift fur Naturforschg, Teil 6a: 32-37 (1951).

7. Daily, John W. "Pulsed Resonance Spectroscopy Applied to Turbulent Combustion Flows," Applied Optics, 15 (4): 955-960 (April 1976).

8. Daily, John W. "Saturation Effects in Laser Induced Fluorescence Spectroscopy," Applied Optics, 16 (3): 568-571 (March 1977).

9. Daily, John W. "Use of Rate Equations to Describe Laser Excitation in Flames," Applied Optics, 16 (8): 2322-2327 (August 1977).

10. Daily, John W. "Saturation of Fluorescence in Flames with a Gaussian Laser Beam," Applied Optics, 17 (2): 225-229 (January 1978).

11. Daily, John W. "Coherent Optical Transient Spectroscopy in Flames," Applied Optics, 18 (3): 360-367 (February 1979).

12. Eckbreth, Alan C., Paul A. Bonczyk, and James F. Verdieck. Review of Laser Raman and Fluorescence Techniques for Practical Combustion Diagnostics. Task I Technical Report, UTRC R77-952665-6. East Hartford, Connecticut: United Technologies Research Center, February 1977.

13. Garcia, Freddie, Jr. The Measurement of Quenching Rate Constants Using Fluorescence Emission. MS Thesis. Wright-Patterson Air Force Base, Ohio: Air Force Institute of Technology, December 1978. (AD A064-055).

14. Gray, Dwight E., coord. ed. American Institute of Physics Handbook (Third Edition). New York: McGraw-Hill Book Company, 1972.

15. Hengehold, Robert L. Introduction to Optical Diagnostics. PH 6.42 Course Notes. Wright-Patterson Air Force Base, Ohio: Air Force Institute of Technology Physics Department, 1981.

16. Herzberg, Gerhard. Molecular Spectra and Molecular Structure, Volume I: Spectra of Diatomic Molecules (Second Edition). New York: Van Nostrand Reinhold Company, 1950.

17. Instruction Manual for the Boxcar Integrator. Model 160. Princeton, New Jersey: Princeton Applied Research Corporation, 1969.

18. Leone, Stephen R. and Kenneth G. Kosnik. "A Tunable Visible and Ultraviolet Laser on S_2 ($B^3\Sigma_u^- - X^3\Sigma_g^-$)," Applied Physics Letters, 30 (7): 346-348 (April 1977).

19. Meyer, Beat, ed. Elemental Sulfur. New York: Interscience Publishers, 1965.

20. Peterson, Drew A. Pure Sulfur Discharges and Associated Spectra. MS Thesis. Wright-Patterson Air Force Base, Ohio: Air Force Institute of Technology, October 1978. (AD A064-762).

21. Peterson, D. A. and L. A. Schlie. "Stable Pure Sulfur Discharges and Associated Spectra," Journal of Chemical Physics, 73 (4): 1551-1566 (August 1980).

22. Piepmeier, E. H. "Theory of Laser Saturated Atomic Resonance Fluorescence," Spectrochimica Acta, 27B: 431-443 (1972).

23. Porterfield, William W. Concepts of Chemistry. New York: W. W. Norton and Company, Inc., 1972.

24. Schreiber, Paul W., Rajendra Gupta, and Won B. Roh. "Application of Lasers to Combustion Diagnostics," Proceedings of the Society for Photo-Optical Instrumentation Engineers (SPIE). 22nd Technical Symposium, San Diego, California, August 1978.

25. Siegman, A. E. An Introduction to Lasers and Masers. New York: McGraw-Hill Book Company, 1971.

26. Smith, W. Hayden. "Absolute Transition Probabilities for Some Electronic States of CS, SO and S_2," Journal of Quantitative Spectroscopy and Radiation Transfer, 9: 1191-1199 (1969).

27. Weichel, Hugo, and Leno S. Pedrotti. Laser Physics I. PH 7.43 Course Notes. Wright-Patterson Air Force Base, Ohio: Air Force Institute of Technology Physics Department, 1981.

28. Wellegehausen, B. "Optically Pumped CW Dimer Lasers," IEEE Journal of Quantum Electronics, QE-15 (10): 1108-1130 (October 1979).

29. Wharton, John J., Jr. Lifetime Measurements Using Fluorescence Emission. MS Thesis. Wright-Patterson Air Force Base, Ohio: Air Force Institute of Technology, December 1977. (AD A055-420).

Vita

Tyrie R. Robbins was born on March 13, 1955 in Chicago, Illinois, and graduated from high school in Chesterton, Indiana in 1973. He attended the United States Air Force Academy in Colorado Springs, Colorado, and graduated with a Bachelor of Science degree in Basic Sciences in 1977. Captain Robbins completed aircraft maintenance officer training at Chanute Air Force Base, Illinois in 1978, and was assigned to 92d Bombardment Wing (SAC) at Fairchild Air Force Base, Washington. While stationed at Fairchild, he served in various positions in the Organizational and Field Maintenance Squadrons. Captain Robbins entered the Air Force Institute of Technology in June 1980.

Permanent address: 1735 Starwood Drive
Chesterton, Indiana 46304

UNCLASSIFIED

SECURITY CLASSIFICATION OF THIS PAGE (When Data Entered)

REPORT DOCUMENTATION PAGE		READ INSTRUCTIONS BEFORE COMPLETING FORM
1. REPORT NUMBER AFIT/GEP/PH/81D-8	2. GOVT ACCESSION NO. AD-A111 141	3. RECIPIENT'S CATALOG NUMBER
4. TITLE (and Subtitle) INVESTIGATION OF LASER INDUCED FLUORESCENCE FOR CONCENTRATION MEASUREMENTS OF DIATOMIC SULFUR		5. TYPE OF REPORT & PERIOD COVERED MS Thesis 6. PERFORMING ORG. REPORT NUMBER
7. AUTHOR(s) Tyrie R. Robbins Captain USAF		8. CONTRACT OR GRANT NUMBER(s)
9. PERFORMING ORGANIZATION NAME AND ADDRESS Air Force Institute of Technology (AFIT-EN) Wright-Patterson AFB, Ohio 45433		10. PROGRAM ELEMENT, PROJECT, TASK AREA & WORK UNIT NUMBERS Project 2301-S1-17
11. CONTROLLING OFFICE NAME AND ADDRESS Aerospace Power Division/POOC-3 Air Force Aero Propulsion Laboratory Wright-Patterson AFB, Ohio 45433		12. REPORT DATE December, 1981 13. NUMBER OF PAGES 71
14. MONITORING AGENCY NAME & ADDRESS(if different from Controlling Office)		15. SECURITY CLASS. (of this report) Unclassified 15a. DECLASSIFICATION/DOWNGRADING SCHEDULE

16. DISTRIBUTION STATEMENT (of this Report)

Approved for public release; distribution unlimited

17. DISTRIBUTION STATEMENT (of the abstract entered in Block 20, if different from Report)

28 JAN 1982

Director of Public
Air Force Institute of Technology (ATC)
Wright-Patterson AFB, OH

18. SUPPLEMENTARY NOTES

Approved for public release; IAW AFR 190-17

Fredric C. Lynch
[redacted]F
[redacted]n

19. KEY WORDS (Continue on reverse side if necessary and identify by block number)

Laser Induced Fluorescence
Diatomic Sulfur
Concentration Measurements

20. ABSTRACT (Continue on reverse side if necessary and identify by block number)

The technique of laser induced fluorescence was used to measure S_2 number densities in a laboratory environment. A rate equation analysis was performed to model transitions within the $B^3\Sigma_u^- - X^3\Sigma_g^-$ system. The $v' = 2$, $v'' = 3$ transition in S_2 at 3290.7 Å was selected for nonresonance fluorescence studies, which included broad spectrum identification, fluorescence intensity

DD FORM 1 JAN 73 1473 EDITION OF 1 NOV 65 IS OBSOLETE

UNCLASSIFIED

SECURITY CLASSIFICATION OF THIS PAGE (When Data Entered)

20. ABSTRACT, Continued

versus temperature and laser power measurements, effective lifetime measurements, and total number density calculations. Data was taken near 600°C to ensure that a large percentage of the sulfur vapor was S_2 ($\geq$ 98%). A pulsed nitrogen laser operating at 3371 Å served as the excitation source for this experiment. Pumping in S_2 occured over the $v' = 2$, $v'' = 4$ transition at 3369 Å due to its near overlap with the N_2 laser line. Experimentally determined number densities were too large in the low pressure region, but generally within one order of magnitude over the 0.3 to 12.6 torr range examined. In concept, laser induced fluorescence proved to be a feasible means of measuring S_2 concentrations. Differences between the known and calculated number densities are attributed to the complexity of S_2, quenching and radiation trapping, difficulties in measuring the effective lifetime, and inadequacies in the rate equation model.

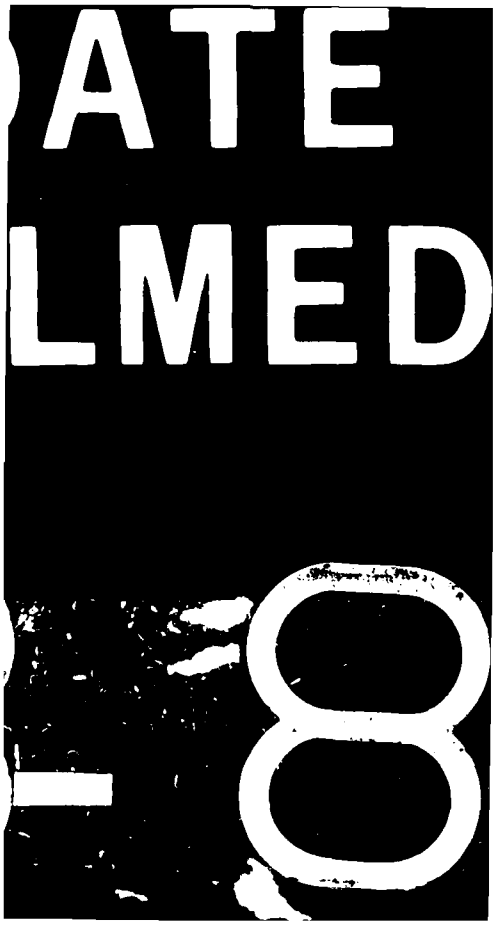
ATE
LMED
18